UNIVERSITEIT VAN PRETORIA
UNIVERSITY OF PRETORIA
YUNIBESITHI YA PRETORIA

Using single molecule spectroscopy to study fast photoprotective processes in plants

by

Joshua Leon Botha

Submitted in partial fulfilment of the requirements for the degree

Magister Scientiae

in the Department of Physics
in the Faculty of Natural and Agricultural Sciences
University of Pretoria
Pretoria

November 2016

UNIVERSITEIT VAN PRETORIA
UNIVERSITY OF PRETORIA
YUNIBESITHI YA PRETORIA

Abstract

Using single molecule spectroscopy to study fast photoprotective processes in plants

by

Joshua Leon Botha

Supervisor:	Dr. T.P.J. Krüger
Co-supervisors:	Prof. Dr. R. van Grondelle, Prof. M. Diale
Degree:	*Magister Scientiae*
Keywords:	photosynthesis, non-photochemical quenching, single molecule spectroscopy, fluorescence intermittency

The fundamental mechanisms involved in photosynthesis provide an opportunity to study physical principles that span over both classical and quantum scales. A better understanding of these mechanisms will benefit the development of alternative energy sources such as cheaper biofuel and more effective photovoltaics. This dissertation describes the single molecule spectroscopy setup that was assembled during my MSc-degree and the underlying theory required to understand the technique, is discussed. The greatest part of the setup development involved customised software development that performs the measurement. The code of this software is briefly discussed. Thereafter the results of a series of single molecule spectroscopy measurements of isolated light harvesting complex II (LHCII) that undergo non-photochemical quenching (NPQ) are described. The fast, reversible, energy-dependent component (qE) of NPQ is emulated by lowering the pH of the solvent in which the complexes are diluted. Apart from fluorescence intensity measurements, time correlated single photon counting is used to measure fluorescence lifetimes, which serves as an indirect measurement of NPQ. It was found that quenching could be taking place before the energy reaches the terminal emitter, and a relationship between intermediate fluorescence states and high jumping frequencies was established.

UNIVERSITEIT VAN PRETORIA
UNIVERSITY OF PRETORIA
YUNIBESITHI YA PRETORIA

Samevatting

Die gebruik van enkelmolekuulspektroskopie om die vinnige fotobeskermende prosesse van plante te bestudeer

deur

Joshua Leon Botha

Studieleier:	Dr. T.P.J. Krüger
Medestudieleiers:	Prof. Dr. R. van Grondelle, Prof. M. Diale
Graad:	*Magister Scientiae*
Kernwoorde:	fotosintese, nie-fotochemiesdowing, enkelmolekuulspektroskopie, fluoressensie-onderbreking

Die fundamentele meganismes wat by fotosintese betrokke is skep 'n ideale geleentheid om beginsels te bestudeer wat oor beide klassieke en kwantumskale strek. 'n Beter verstaan van hierdie meganismes sal die ontwikkeling van alternatiewe energiebronne soos goedkoop biobrandstof en meer effektiewe fotovoltaïese selle bevorder. Hierdie verhandeling beskryf die enkelmolekuulspektroskopie-opstelling wat tydens my MSc-graad opgerig is en die onderliggende teorie wat nodig is om die tegniek te verstaan, word bespreek. Die grootste deel van die ontwikkeling van die opstelling het die ontwikkeling van toepassingsgerigte sagteware behels. Die kode van hierdie sagteware word oorsigtelik bepreek. Vervolgens word die resultate van 'n reeks enkelmolekuulspektroskopie-metings beskryf waartydens nie-fotochemiesedowing (NFD) in die geïsoleerde ligversamelingskompleks II (LHCII) van hoër plante bestudeer is. Die vinnige, omkeerbare, energie-afhanklike komponent (qE) van NFD is geëmuleer deur die pH van die oplossing waarin die komplekse opgelos is, te verlaag. Buiten metings van die fluoressensie-intensiteite is tydsgekorreleerde enkelfotontelling ook toegepas om fluoressensieleeftye te meet, wat as 'n indirekte meting van die mate van NFD dien. Die moontlikheid dat dowing plaasvind voordat die opwekkingsenergie die laagste energietoestand in die kompleks bereik, is ontdek en 'n verwantskap tussen intermediêre fluoressensietoestande en hoëfrekwensieskakeling word gelê.

Declaration

I, Joshua Leon Botha declare that the dissertation, which I hereby submit for the degree *Magister Scientiae* at the University of Pretoria, is my own work and has not previously been submitted by me for a degree at this or any other tertiary institution.

Signature: .....

Joshua Leon Botha

Student number: 13290152

Date: Sunday 27th November, 2016

Acknowledgments

Thank you Dr. Krüger for all your patience, guidance, long-suffering, and unending support in all things – academic and non-academic. For financial support I thank Prof. Diale, Prof. Malherbe and the NRF. I also thank SAVUSA for enabling my work at the Vrije Universiteit of Amsterdam.

How does one measure the cost of the sacrifice parents make to give their children opportunities they did not have? Thank you Leon and Karin Botha for your love and support. Thank you to all my friends and family that have supported me and put up with all my ramblings about almost being done! To the love of my life, my wife Christa: thank you for being a student with me, for being there when I was close to giving up, and pointing me to my strength when I thought I had lost it. And the crescendo of my thankfulness goes to our Saviour Jesus Christ.

UNIVERSITEIT VAN PRETORIA
UNIVERSITY OF PRETORIA
YUNIBESITHI YA PRETORIA

Dedications

I dedicate this dissertation to my father and mother, Leon and Karin Botha.

UNIVERSITEIT VAN PRETORIA
UNIVERSITY OF PRETORIA
YUNIBESITHI YA PRETORIA

"Research is to see what everybody has seen and think what nobody has thought."

- Albert Szent-Györgyi

UNIVERSITEIT VAN PRETORIA
UNIVERSITY OF PRETORIA
YUNIBESITHI YA PRETORIA

Contents

UNIVERSITEIT VAN PRETORIA
UNIVERSITY OF PRETORIA
YUNIBESITHI YA PRETORIA

UNIVERSITEIT VAN PRETORIA
UNIVERSITY OF PRETORIA
YUNIBESITHI YA PRETORIA

List of Figures

UNIVERSITEIT VAN PRETORIA
UNIVERSITY OF PRETORIA
YUNIBESITHI YA PRETORIA

UNIVERSITEIT VAN PRETORIA
UNIVERSITY OF PRETORIA
YUNIBESITHI YA PRETORIA

Chapter 1

Theoretical Background

All things need to start somewhere, and in this case an adequate place to start is at the *beginning*. One could say life is intricate and complex, nonetheless it obeys the laws of physics. It follows that it should be possible to describe life by using the fundamental principles of physics. However, this turns out to be no trivial task due to the complexity of the processes involved in life. Towards this end it would be logical to first define what is meant by *life*, followed by breaking it down into its fundamental units. To attempt this would be ambitious. Instead this dissertation will investigate only a small, yet imperative, section of life: photosynthesis. More accurately, this study is an investigation into the first steps of photosynthesis that take place in plants.

Why photosynthesis? It is well-known that for survival – which may be considered to be synonymous with life – there needs to be some source of energy. All possible sources of energy for life on earth could be divided into one of two camps: terrestrial and extraterrestrial. Although there are sources that originate on earth they are few and not easily accessible. While it is true that terrestrial

energy sources[1] do sustain some forms of life[2], these organisms are completely outnumbered by those that rely (directly or indirectly) on extraterrestrial energy sources. Unequivocally the most predominant extraterrestrial source is the electromagnetic radiation as provided by our local star. Keeping this in mind it is intuitively simple that the primary source for most life on earth would be solar energy. Surprisingly, only a single natural mechanism exists by which solar energy is captured and stored for use in living organisms: photosynthesis. Defined by the absorption of light to effectuate the oxidation of water (in oxygenic photosynthesis) or hydrogen sulfide (in anoxygenic photosynthesis) which in turn drives the formation of carbon-carbon bonds, photosynthesis is achieved in mechanistically varied ways.

The earth is irradiated with 120 000 TW of electromagnetic radiation by the sun. In contrast, the human global energy usage has been suggested to be approximately 13 TW [3]. One estimation of the rate at which energy is successfully converted into biomass by photosynthesis is approximately 130 TW [4]. This comparison serves as a testimony to the success of photosynthesis as a source of energy for life. It also serves as a strong motivation for understanding the mechanisms and processes involved in photosynthesis. Mankind's energy problems would be dealt with if we could capture and store solar energy to the same extent.

One of the interesting facets of photosynthesis is that it is optimised for low solar intensities. While at first this might seem counterintuitive one needs only to envisage a situation in which an organism is exposed to overcast weather for extended durations on end. It then becomes apparent that being able to survive in unfa-

[1] An example of such a terrestrial energy source is nuclear fission, that has been confirmed to account for more than half of the heat of our planet [1].

[2] Bacteria have been found living 2,8 km below the surface of the earth that survive by sustainably metabolising geo-radioactively produced sulfate and hydrogen [2]

UNIVERSITEIT VAN PRETORIA
UNIVERSITY OF PRETORIA
YUNIBESITHI YA PRETORIA

vourable conditions is of a higher priority than being able to utilise high light conditions to the greatest possible extent. Consequently, photosynthesis needs to be highly light sensitive. This, however, introduces an unintended difficulty: damage due to excessive energy absorption becomes a very real probability. In fact, in sunny weather higher plants reach this point soon after sunrise. In answer to this photosynthetic organisms enter an energy dissipative state throughout the day. After absorption of a photon, before the energy is utilised, the energy is rapidly and safely *dumped* as heat. Photosynthesis has the ability to *decide* to switch between a light harvesting state and an energy dissipative state depending on light conditions. Many questions of how this remarkable feat is achieved remain unanswered.

1.1 The Basics of Photosynthesis

Photosynthesis in plant cells takes place in organelles called chloroplasts. These are membrane enclosures filled with a fluid, called the stroma, and bilipid membrane structures called thylakoids. Thylakoid membranes enclose a fluid called the thylakoid lumen. Results from electron microscopy and other imaging techniques have shown extensive folding of thylakoid membranes that form two distinct domains: stacked thylakoid membranes called grana, and unstacked thylakoid membranes that connect the grana, called stroma lamellae [5]. The first processes of photosynthesis (in plant cells) take place in thylakoid membrane-bound proteins, those of importance being Photosystem I & II (PSI & PSII), ATP synthase and cytochrome b_6f complex (refer to fig. 1.1). It has been shown that the grana contains most of the PSII whereas the stroma lamellae contain most of the PSI and ATP synthase. The cytochrome b_6f complexes are evenly distributed between the

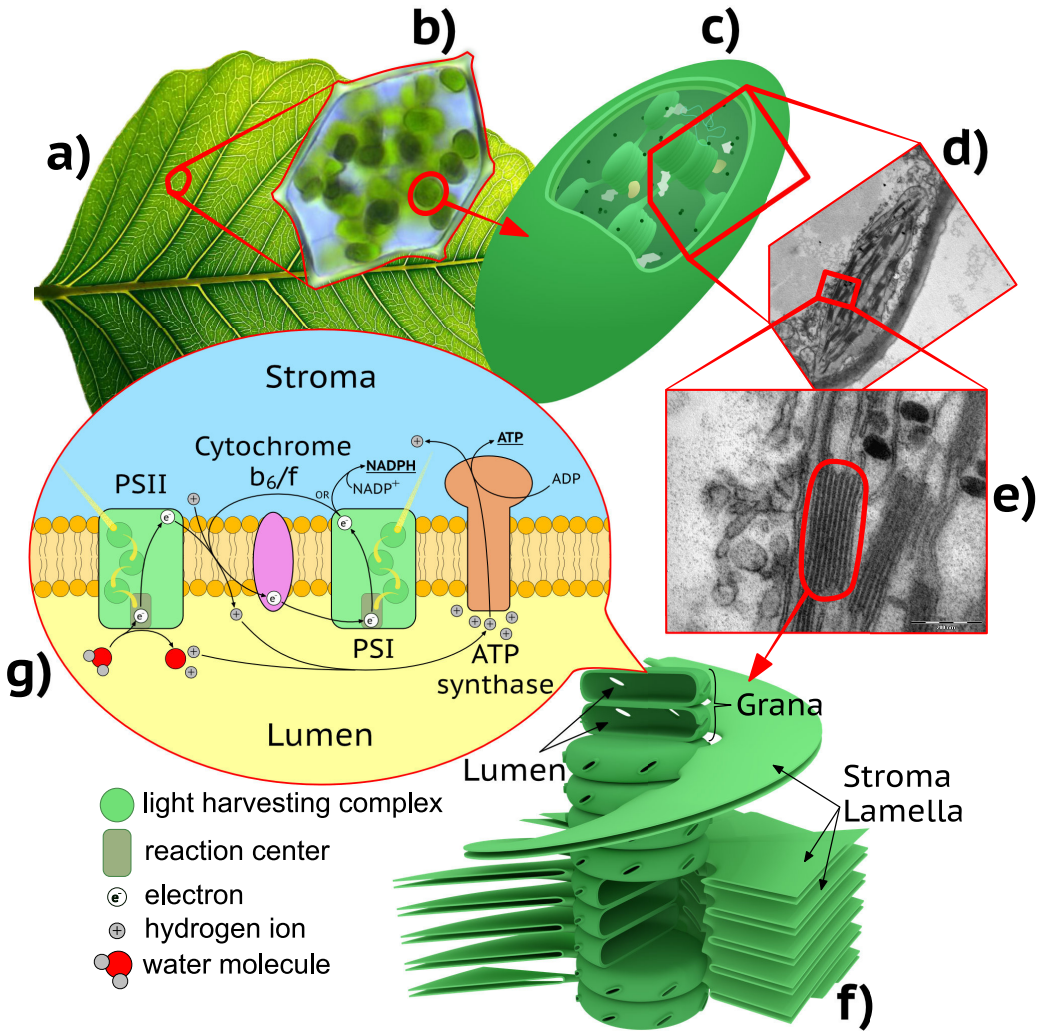

Figure 1.1: From **a)** a photo of a leaf, to **b)** a microscope photo of a plant cell, to **c)** a illustration of a chloroplast, to **d)** a 12000x and **e)** a 30000x transmission electron microscope image of a chloroplast, to **f)** illustration of a thylakoid, and finally to a **g)** illustration of a thylakoid membrane. The thylakoid **f)** was first proposed to have a helical spiral structure in 1970 [7]. Sections of the stroma lamellae in **f)** have been cut out to reveal the manner in which they connect to the grana stacks. Illustration **g)** includes membrane proteins involved in the light-dependent steps in photosynthesis such as PSI & PSII that contain light harvesting complexes and reaction centres. Note that the illustration does not hold true to the actual stoichiometric factors. Image **b)** was adapted from Kristian Peters, images **d)** and **e)** were adapted from and3k and caper437, and **c)** and **f)** was adapted from Kelvinsong, all under CC BY-SA 3.0.

two domains [6].

Photosynthesis comprises two sets of processes, the light-dependent and the light-

independent processes. In the light-dependent phase photons are absorbed by any of the approximately 200 pigment molecules found in each PSI and PSII. Once a photon is absorbed by one of the pigments in PSII the energy undergoes excitation energy transfer (EET) between pigment molecules of PSII and eventually reaches a complex known as the reaction centre (RC). A special pair of pigment molecules is then excited and generates a free electron. The electron is transported to the other side of the membrane resulting in a charge separation which prevents charge recombination. The electron vacancy is filled sequentially by a series of redox reactions and eventually oxidises an enzyme called the oxygen evolving complex (OEC). With each subsequent absorption of a photon, another electron is taken from the OEC. After four[3] successful charge separations the OEC reacts with two water molecules to produce four hydrogen ions, and an oxygen molecule. This can be represented by

$$\begin{aligned}
\text{photon} + \text{OEC} &\longrightarrow e^- + \text{OEC}^{+1} \\
\text{photon} + \text{OEC}^{+1} &\longrightarrow e^- + \text{OEC}^{+2} \\
\text{photon} + \text{OEC}^{+2} &\longrightarrow e^- + \text{OEC}^{+3} \\
\text{photon} + \text{OEC}^{+3} &\longrightarrow e^- + \text{OEC}^{+4}
\end{aligned}$$

followed by

$$2H_2O \xrightarrow{\text{OEC}^{+4}} 4\,H^+ + 2\,O_2$$

or in short

$$4\,\text{photons} + H_2O \xrightarrow{\text{OEC}} 4\,H^+ + 2\,O_2 + 4\,e^-$$

The free electrons supplied by this process are transported in an electron transport chain, as represented by fig. 1.1g. In the first step the excited electron is transported to cytochrome b_6f and in the process two protons are transported from the

[3] In dark-adapted PSII systems the OEC complex resides in the OEC^{+1}, in which case only three excitation would be required to oxidise water.

UNIVERSITEIT VAN PRETORIA
UNIVERSITY OF PRETORIA
YUNIBESITHI YA PRETORIA

stroma to the lumen. PSI acts similarly to PSII, the difference being that electrons are supplied from cytochrome b_6f as part of the electron transport chain, and not from splitting water. The fate of the electron excited in PSI after being transported to the stromal side of the membrane is either to cycle back to cytochrome b_6f or to reduce $NADP^+$ to NADPH which is a stable and mobile energy carrier. As part of the process of cycling back to cytochrome b_6f two additional hydrogen ions are transported from the stroma to the lumen. The build-up of hydrogen ions due to water splitting at PSII and the electron transport chain results in the build-up of a transmembrane proton gradient. It is the proton gradient that ultimately drives ATP synthase to form ATP from ADP – which is the basic cellular energy unit. Consequently, the resulting products of the light dependent reactions are NADPH, ATP and molecular oxygen, the latter being a byproduct that is released into the atmosphere. In the light-independent phase ATP and NADPH in the stroma are used to create carbon-carbon bonds in molecules (carbohydrates) though a carbon fixation process called the Calvin Benson Cycle. Eventually the energy captured by photosynthesis is stored in sugars to be transported and used throughout the plant.

As previously mentioned, photosynthetic organisms often need to protect themselves against overexposure to light. Processes that effectuate this self-protection are collectively known as photoprotection processes and take place over many timescales, from seconds to hours and even years. Some of these processes are attributed to a phenomenon called non-photochemical quenching (NPQ). The energy-dependent component (qE) of NPQ takes place just after the energy absorption [8].

In the light-dependent phase of photosynthesis the process of initial energy absorption and metastable energy storage has a quantum efficiency of virtually 100%

UNIVERSITEIT VAN PRETORIA
UNIVERSITY OF PRETORIA
YUNIBESITHI YA PRETORIA

when exposed to a sufficiently low photon flux. This is to say that the energy of every photon that is absorbed is used in photosynthesis. In high light conditions the rate of energy absorption is greater than the rate at which the energy is used. In oxygenic photosynthesis the excess energy forms chlorophyll triplets which in turn react with molecular oxygen to form oxygen radicals that are highly reactive and toxic to living organisms [9]. Oxygenic photosynthetic organisms therefore have to be able to protect themselves in high light conditions and achieve this through NPQ that limits the formation of oxygen radicals. To understand how this is done one could take a closer look at PSII, where qE has been shown to take place.

1.2 Structural Context

On the level of proteins, there is a strong correlation between structure and biological function. For this reason the protein structural context of photosynthesis must be known before the dynamics involved can be understood.

The PSII supercomplex consists of the RC, minor antennae and LHCII. Various studies have resolved the structure of PSII complexes found in cyanobacteria to resolutions of 10 Å to <3 Å [12–16], as well as a recently resolved PSII structure from spinach at 3,2 Å [17]. The PSII-supercomplex was found to consist of various subunits (see fig. 1.2). One noteworthy type of subunit is the peripheral antenna complexes that absorb and transfer energy to the core PSII units that contain RCs. The example in fig. 1.2 is referred to as the $C_2S_2M_2$ supercomplex, which refers to it consisting of two core subunits, two strongly bound and two medium-strength bound LHCII complexes. Two types of peripheral antenna complexes are found, the most abundant being light harvesting complex II (LHCII).

The second type are minor antenna complexes, of which there are three variations: CP29, CP26 and CP24. LHCII and CP29 have been resolved separately using X-ray crystallography [18–20], and CP26 and CP24 are similar to CP29 structurally, based on the recently resolved structure of the PSII-supercomplex [17]. The core consists of the RC and two types of antenna complexes, CP43 and CP47, which both have efficient energy transfer pathways to the RC. During qE an additional quenching channel is opened for the energy absorbed by pigment molecules to be siphoned off and released as heat before it can lead to radical oxygen formation. This quenching most likely takes place in LHCII [21–24]. Crystal structures [18] have revealed that LHCII consists of three identical protein subunits that form a trimeric complex, as well as fifty-four pigment molecules – which consist of chlorophylls and carotenoids – kept in place by the protein scaffolding [17] (see fig. 1.3).

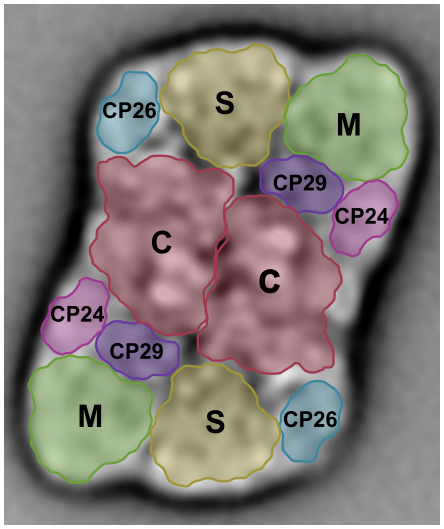

Figure 1.2: Image of a PSII supercomplex with an overlaid projection of subcomplexes. Image adapted from [10] and overlaid projection taken from [11]. The two red *C* areas indicate the two core subunits. The pink *CP24*, blue *CP26* and purple *CP29* are monomeric peripheral antena, while the green *M* and yellow *S* regions indicate a moderately and strongly coupled trimeric LHCII complex respectively. Additional LHCII complexes can bind to the superstructure and thereby increase the absorption cross-section of the supercomplex.

1.3 Light Interaction and Dynamics

Energy delocalisation between adjacent pigments in LHCII – called excitons [25] – results in highly efficient energy transfer within LHCII [26]. Consequently, upon photon absorption by one of the pigments in LHCII the excitation typically quickly relaxes to the site with the lowest energy and remains there until it meets one of a few de-excitation fates, as depicted in fig. 1.4. Energy transfer between complexes within PSII supercomplexes (as in fig. 1.2) have also been found to be highly efficient. This means that as long as the complex that has absorbed the photon is in the vicinity of other complexes – of which some would include RCs –

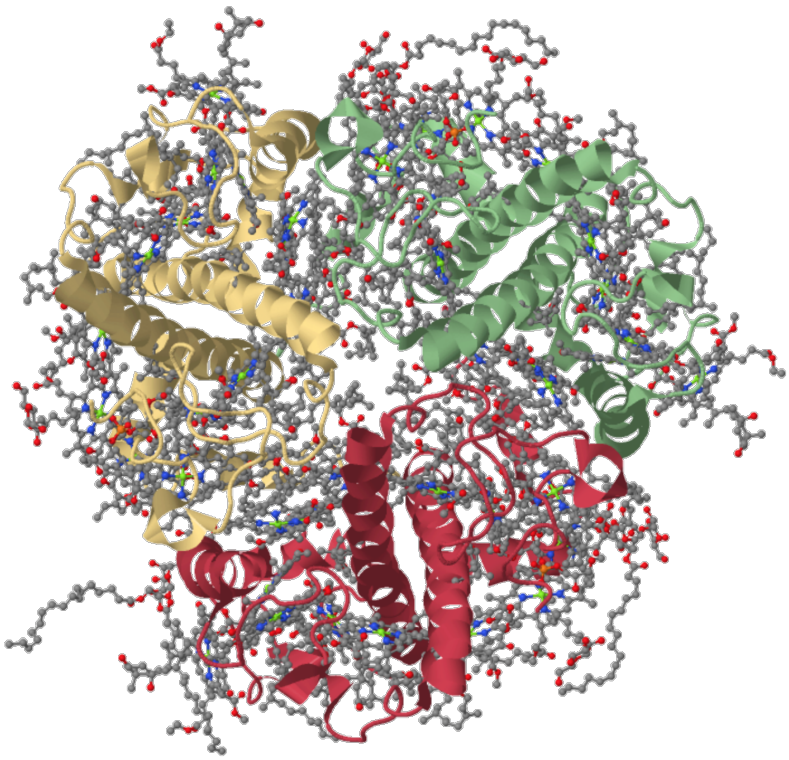

Figure 1.3: Light harvesting complex II as resolved by [18] (available on PDB under ID 1RWT) and rendered by JMol. Each colour ribbon represents a monomeric protein scaffold. The remaining ball-and-stick molecules represent the chlorophyll and carotenoid pigments.

the transfer to a RC is the predominant process that has the highest probability of occurring. The average rate at which an excitation reaches a fate is governed by the rate equation

$$k_L = \overbrace{\underbrace{k_R + k_{ISC} + k_{IC} + k_q}_{\text{Isolated}} + k_{RC}}^{\text{Coupled to neighbouring complexes}} \tag{1.1}$$

where $1/k_L = \tau_L$ is the lifetime of the excitation. The rate at which excitations are radiatively dissipated is given by k_R. The excitation could also result in electron spin flip (intersystem crossing), resulting in an electronic triplet state. The rate at which this happens is given by k_{ISC}. Additionally, k_{IC} is the rate at which non-radiative de-excitation through vibrational levels while preserving spin takes place.

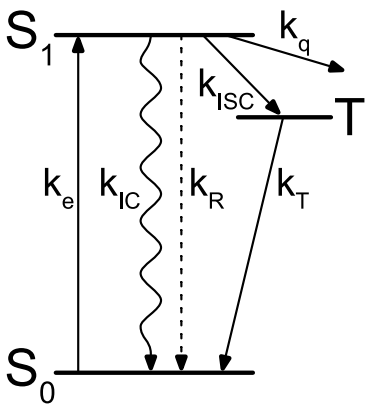

Figure 1.4: Chlorophyll Jablonski excitation fate diagram. S_0 and S_1 represent the electronic ground state and first excited state respectfully. k_e is the rate at which excitations are introduced into the system. k_R is the rate at which the excitation is radiatively emitted in the form of fluorescence, and k_{ISC} is the rate at which the energy leads to spin flip of an electron. The triplet states decay at a rate given by k_T, however, this rate does not affect the rate at which S_1 is depopulated, but rather affects the rate at which the S_0 is repopulated. Lastly, k_q is the rate at which excitations are quenched due to qE.

The three processes mentioned – k_R, k_{ISC} and k_{IC} – are intrinsic to the structure of the complex and their average rates can therefore be seen as constant. The rate of quenching due to qE (if present in the system) is given by k_q. Lastly, the rate at which energy is transferred to the RC is given by k_{RC}. When considering that k_{RC} is not present in isolated LHCII complexes it becomes apparent that an indirect measurement of the rate of quenching present in the system (k_q) can be made by measuring the effective fluorescence lifetime (τ_L).

The quenching channel due to qE in the system is regularly switched on and off. This reversible quenching has been shown to be related to a phenomenon known as fluorescence intermittency [27]: abrupt and large changes in the fluorescence

UNIVERSITEIT VAN PRETORIA
UNIVERSITY OF PRETORIA
YUNIBESITHI YA PRETORIA

intensity of isolated LHCII complexes under continuous illumination. Fluorescence intermittency – also known as blinking – was first observed in single dye molecules [28] and later also found in quantum dots [29]. Interestingly, complex systems such as pigment-protein complexes were found to exhibit the same behaviour [30]. The precise mechanism that is involved has yet to be confirmed for protein complexes, however. It is the attempt of this thesis to shed additional light on how blinking is linked to qE.

This concludes the contextual theoretical discussion. The chapter that follows concerns the theory involved in single molecule spectroscopy, as well as a technical discussion of the equipment used. Chapter 3 is a brief discussion on the software that orchestrates the measurement process. It has the intent of equipping the reader with a basic understanding of the code in order to improve on – or develop – additional features. The data collected is then presented in chapter 4, and conclusions drawn therefrom discussed. The dissertation then ends with a short summary in chapter 5.

UNIVERSITEIT VAN PRETORIA
UNIVERSITY OF PRETORIA
YUNIBESITHI YA PRETORIA

Chapter 2

Single Molecule Spectroscopy

The scientific process is one that builds on the foundation of what has been done before. In the same way the study of photosynthetic processes has built on what has already been established. However, as our understanding grows in depth and purview, so too do the techniques of investigation that have brought us thus far need to adapt and improve to enable further progress. Ensemble measurements of LHCII have been used extensively to, amongst other things, gain insight into the energy dynamics within the protein. However, these types of measurements average over all the complexes measured and only single mean values are obtained. In contrast, to make a useful study of phenomena such as fluorescence intermittency, single complexes can be measured one after the other to build up a set of individual values and thereby incorporate distribution information in the results. This is the most important advantage that single molecule spectroscopy (SMS) offers when compared to ensemble spectroscopy, and for this reason SMS is ideal for studying quenching mechanisms in LHCII. This chapter covers the basic theories involved in SMS, as well as a detailed description of the SMS setup that was constructed.

UNIVERSITEIT VAN PRETORIA
UNIVERSITY OF PRETORIA
YUNIBESITHI YA PRETORIA

2.1 Theory

Before using the tools-of-the-trade it will do well to first reflect on the theoretical aspects involved in SMS. Toward this end a brief discussion on the limitation set upon us by the nature of light follows. Thereafter comes a description of the spectroscopic method used to reduce noise during measurements. Lastly, we look at how SMS will be applied to investigating the quenching dynamics of LHCII.

2.1.1 Diffraction Limit

To investigate individual molecules understanding the concept of a diffraction limited focal spot is a good starting point. In microscopy, the Abbe diffraction limit – as defined by Ernst Abbe in 1873 – is a theoretical limit to how tightly a beam of light can be focused. Consider a plane wave of light where each point on the wavefront can be seen as a point source for a new wavefront expanding in all directions. The superposition of all these waves results in a forward propagating light wave. When such a light wave is disturbed by an edge the usual superposition is incomplete, and the result is no longer a forward propagating plane wave. Instead the *'point sources'* nearest the edge result in the light wave expanding past the edge in directions no longer parallel to the propagation direction of the plane wave. It therefore seems as if the light *bends* around the edge. This is known as the Huygens-Fresnel principle. One of the results of this property of light is that light being focused by a perfect lens cannot result in an infinitely small point at the focal plane, instead, a three dimensional diffraction pattern is formed.

Consider an infinitely small point source of light at the focal plane incident on a lens. The light from the point source would not - when focused by the lens - appear as an infinitely small spot. Instead it undergoes a three dimensional spatial

UNIVERSITEIT VAN PRETORIA
UNIVERSITY OF PRETORIA
YUNIBESITHI YA PRETORIA

transformation which is defined by the point spread function (PSF) of the optical system. In the case of a diffraction limited beam the diffraction pattern that forms at the focal plane is described by the PSF of the optical system. A cross section of the PSF at the focal plane would reveal the smallest two-dimensional diffraction pattern obtainable. The 1st order maximum spot of the diffraction pattern is called the Airy disk and has a radius to the 1st order minimum given by

$$r \approx 0.61 \frac{\lambda}{n \sin \theta} \tag{2.1}$$

where λ is the wavelength of the light, n is the refractive index of the medium the light is traveling through, and θ is the semi-aperture angle (also called the half angle of the light cone) as illustrated in fig. 2.1. The product $n \sin \theta$ depends only on the objective and is known as the numerical aperture (NA). Modern objectives can achieve an NA of between 1,4 - 1,6. The objective used in our experimental setup has a NA value of 1,45, which means that eq. (2.1) can be approximated by

$$d \approx \frac{\lambda}{2{,}4} \tag{2.2}$$

such that for a wavelength of 630 nm, as an example, the smallest Airy disk that can be achieved will have a radius of ~260 nm. Consequently, any object smaller than this limit is too small to be investigated on a single unit level in conventional spectroscopic methods based on light. Unfortunately proteins have a size in the order of a couple of nanometers, considerably smaller than the diffraction limit. Therefore in using light to measure single proteins they have to be isolated from other proteins by at least a couple hundreds of nanometer in the focal plane. It must also be mentioned that the measured section is not that of a surface, but of a volume. This volume can be visualised as two cones of light joined at the focal plane, small end to small end, with the Airy disk radius at the

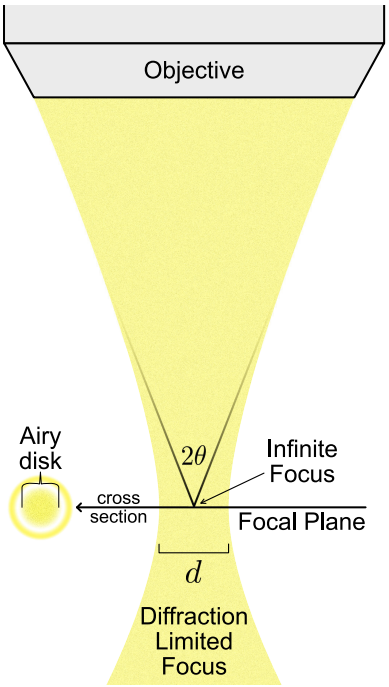

Figure 2.1: Diffraction limited beam as focused by a perfect microscope objective. The focal plane is the plane at which the beam is most focused. The first maximum lobe of the resulting diffraction pattern is referred to as the Airy disk. A cross section at this point reveals the two dimensional PSF. The spot diameter depends on the wavelength of the light and resolving power of the objective.

joint. The cones then spread out on the axis of the light propagation, up until the photons reach a density small enough that the probability of exciting a protein or impurity is negligible. The resulting volume is referred to as the detection volume, as illustrated by fig. 2.2. Consequently, to enable the measurement of a single protein only one protein should be found in the detection volume at any given time. Additionally, as impurities are always present it follows that the amount of noise due to impurities is directly related to the size of the detection volume.

To achieve having only one protein in the detection volume two strategies can be considered. Both methods share one commonality; to ensure that it is possible to only have one protein in the detection volume the concentration of proteins in a solution must be low enough that the average distance between proteins is larger than the dimensions of the detection volume. However, the two methods differ in how they ensure that the duration of the measurement of one protein does not depend on random moments that a protein happens to diffuse into the detection volume, as that would typically last only a few milliseconds. The first strategy is to immobilise the proteins, and the second is to track and follow the proteins in three dimensions as they diffuse. The latter method presents a technological challenge much greater than that of simply confining the protein, and has subsequently not been the method of choice in the past for studying individual LHCIIs. Instead

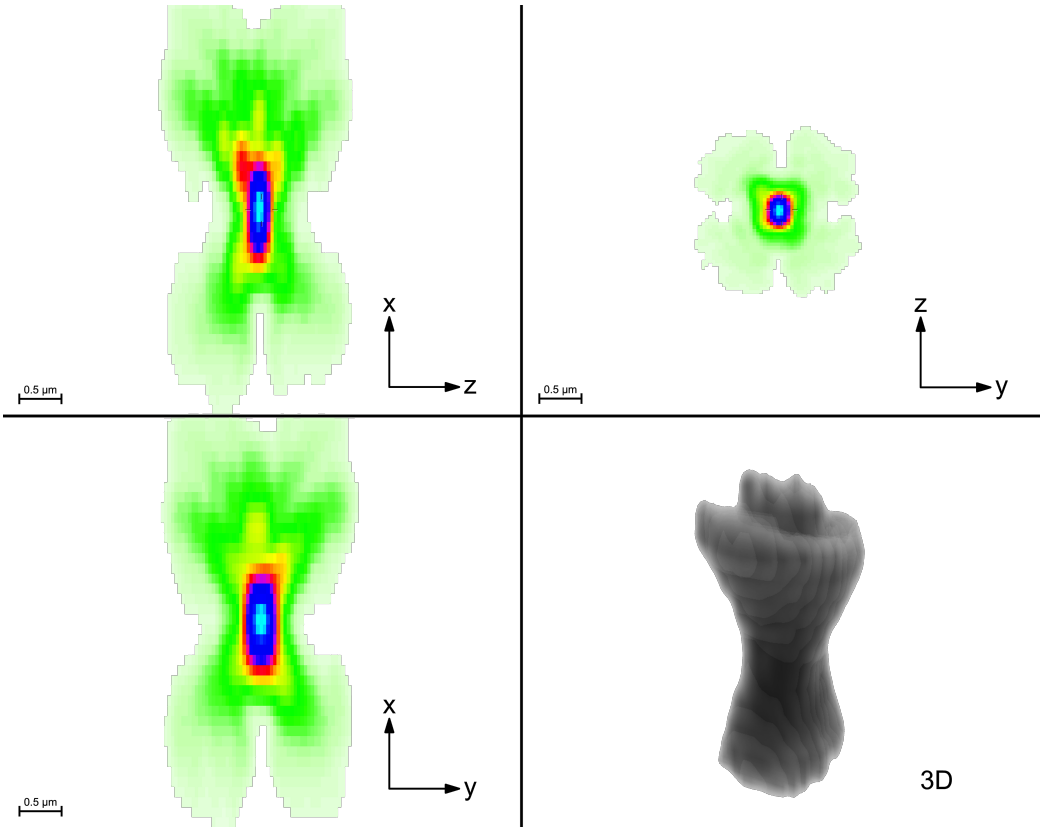

Figure 2.2: Example of an experimentally derived PSF from a confocal microscope using a 63x 1,4 NA oil objective. Shown are views in the x-z plane, x-y plane, y-z plane and a 3D representation. Images of 100 nm beads were used to generate this PSF by using Huygens Professional software. Adapted from Howard Vindin under CC BY-SA 4.0.

the complexes typically are made to bind to a glass surface that has been treated with a binding agent. It is then trivial to satisfy the isolation requirement at the focal plane by choosing a dilution factor high enough that the case of two proteins binding within a distance of a few hundreds of nanometer of each other is improbable. One advantage of this method is that the concentration of proteins in the solution will be sufficiently low that, so that when proteins do diffuse into the detection volume, the measurement will be small and infrequent enough to not be a problem. Following the protein in free diffusion has consequently been proposed to have the advantage of providing measurements that are more accurate

when compared to proteins in their natural environments as the proteins are not subjected to surface adhesion forces.

2.1.2 Confocal Microscopy

One of the inherent challenges that needs to be faced when optically observing a single protein is that the fluorescence emitted is small when compared to the sensitivity of the most sensors. Fluorescence – a natural phenomenon – is the re-emission of absorbed electromagnetic radiation (see fig. 2.3). A molecule absorbs a photon and an electron is excited to a higher electronic state. Some of the energy is lost through non-radiative processes such as dynamic collisional quenching, resonance energy transfer (near-field dipole-dipole interaction), internal conversion, and intersystem crossing. The probability exists that after some time (typically in the nanosecond regime) the system will return to the ground state by the emission of a photon in a direction that is dependent on the dipole moment at a wavelength slightly longer than that of the absorbed photon. The probability that the absorbed energy will indeed be fluoresced is governed by the rate at which quenching takes place through other channels (refer to section 1.3), and for LHCII this probability is 22 % ± 3 %, and the fluorescence lifetime (i.e. the duration after which $1/e$ of the emissions occur) of LHCII is 4,00 ns ± 3 % [31]. When

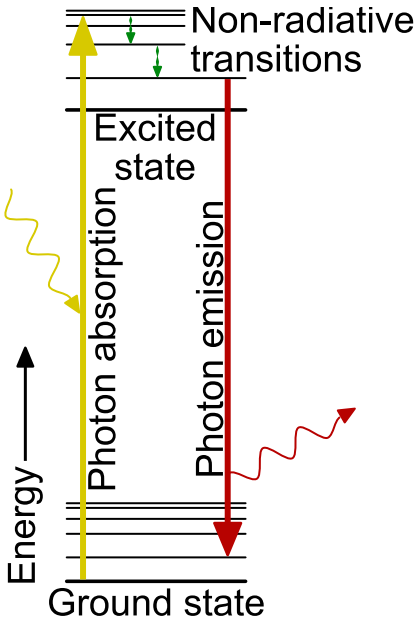

Figure 2.3: Fluorescence energy loss diagram. The excited states referred to can be different electronic states, or in most cases are different vibrational states within the same electronic state. Non-radiative processes result in a loss of energy before a photon is emitted. For this reason the fluoresced light usually has a longer wavelength than that of the absorbed light.

observing a single LHCII protein the resulting fluorescence intensity is small in comparison to that of the light used to excite it. For this reason highly sensitive photon detectors need to be used. However, the photon intensity emitted from the complex in question also needs to be sufficiently larger than the background noise present in the optical system.

Towards reducing background noise the principle of confocal microscopy can be implemented, thereby increase the signal to noise ratio (SNR) of the fluorescence signal. Figure 2.4 is an illustration of the confocal principle. Light that will eventually excite the molecule is first reflected by a dichroic beam splitter, that acts

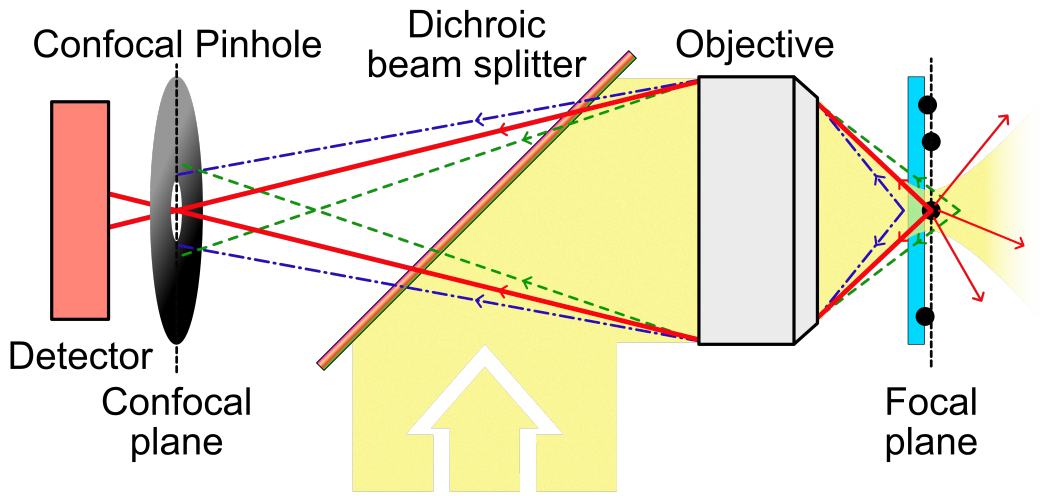

Figure 2.4: Confocal microscopy illustration. The large yellow beam indicates the light used to excite the sample molecule, which in turn results in fluorescence. The dichroic mirror reflects short wavelengths and transmits longer wavelengths as defined by a cut-off wavelength inherent in its design (see section 2.2 on page 24). The objective focuses the light to a diffraction limited spot at the focal plane. If a sample is in the detection volume some of the resulting fluorescence will be captured by the objective. The solid red lines indicate fluorescence from the sample molecule at the focal plane in the focused spot. The dashed green lines illustrate the path light would follow if the source were to be directly before the focal plane, and the dotted blue light just after. The dashed green and dotted blue lines show possible light sources that would increase the background noise and would ideally be prevented from being added to the measurement. The light directed back through the objective then reaches the dichroic mirror, and if the wavelength of the light is longer than the cut-off wavelength it is transmitted the second pinhole. This pinhole acts as a secondary focal plane, or confocal plane. Only the light originating from the focal plane is allowed to pass through and reach the detector.

UNIVERSITEIT VAN PRETORIA
UNIVERSITY OF PRETORIA
YUNIBESITHI YA PRETORIA

as a long-pass filter. This means that for wavelengths longer than a specified wavelength, called the cut-off wavelength, the light will be reflected whereas shorter wavelengths will be transmitted. The light is then focused by the objective to a diffraction limited spot at the focal plane. If a protein is excited at the focal plane a fraction of the fluorescence is emitted toward the objective and subsequently directed back toward the dichroic beam splitter. The cutoff wavelength of the dichroic mirror is therefore chosen such that the excitation beam will be reflected toward the sample, as well as to ensure that most of the resulting fluorescence will be transmitted. The fluorescence is then focused onto a pinhole. This pinhole acts as a second 'focal plane', or confocal plane, allowing only light that originated at the focal plane to pass through. If there were to be some other sources of light before or after the focal plane in the path of the excitation light, such as fluorescing impurities or other proteins molecules, their fluorescence would be incident on the pinhole surface. Using this method is crucial in allowing fluorescence from a single molecule to have a sufficient intensity as to be distinguishable from the background noise in the optical system.

2.1.3 Fluorescence Measurements of Single LHCII

The aim of SMS of an LHCII complex is to extract useful information (such as energy dynamics and/or structural properties) from the measurement of a stream of fluoresced photons. Two classes of information can be extracted: the fluorescence distribution information (i.e. the intensity and wavelength of the fluorescence), and the fluorescence lifetime. The former can easily be measured by implementing a single photon avalanche diode (SPAD), which can typically have a dark count in the order of 20 counts per second with response times in the order of 100 ns, as well as a highly sensitive CCD camera for the spectral information. This has been successfully achieved numerous times [32–35]. Fluorescence life-

time measurements can be made by implementing time correlated single photon counting (TCSPC). In this method single photons are detected, and the subsequent arrival time information is stored. For systems where laser pulses are used to excite the sample the relative photon arrival times after excitation are calculated by comparing the absolute arrival time of each photon to that of the absolute laser pulse times. The result is that both the relative and absolute photon arrival times are known.

Past studies of single fluorescing molecules in which fluorescence intensity over time was measured have revealed a phenomenon which has been called fluorescence intermittency. Large, abrupt, seemingly stochastic changes in fluorescence intensity suggest that these systems consist of two distinct fluorescing states. Commonly referred to as *on* and *off* states, the system can stay in *on* state for some time before switching to the *off* state.

2.2 Experimental Setup

In the discussion of the experimental SMS setup, which was built from the ground up, fig. 2.5 will be used as guideline. Refer to fig. B.7 and fig. B.8 for photographs of the setup. Each component will be discussed in the same order as the light would follow.

Light Source

As a source of light a Fianium Supercontinuum laser (C400-4-PP) is used. This fibre based laser emits an ultra broadband supercontinuum beam of light that has a spectrum ranging from approximately 420 nm to 2200 nm. The laser has a fun-

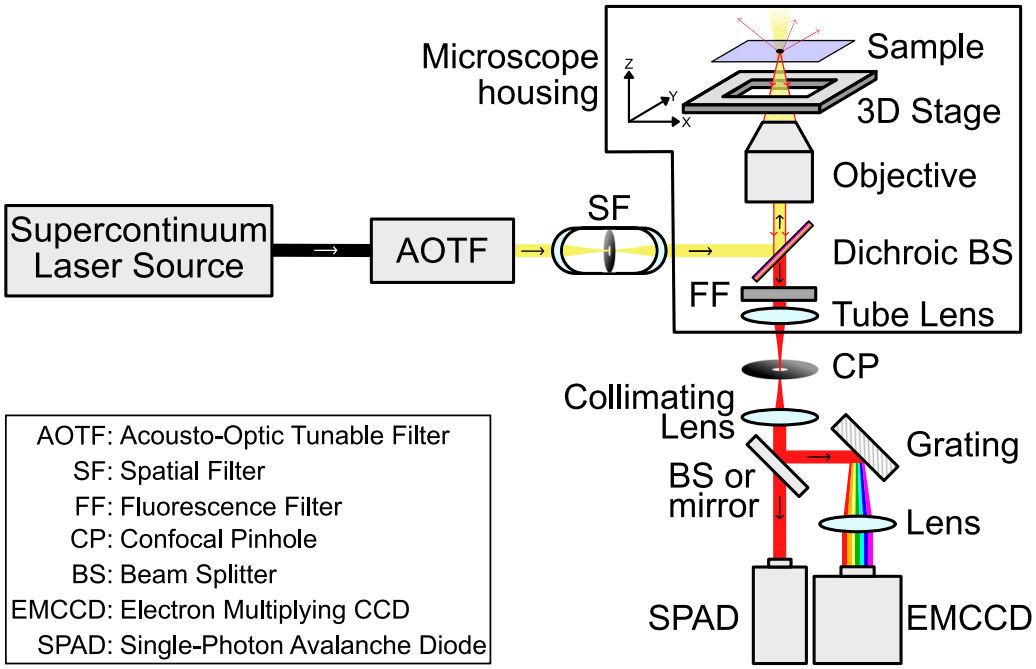

Figure 2.5: A simplified illustration of the experimental SMS setup built.

damental pulsewidth of 6 ps and has a selectable pulse repetition rate of between 0,1 MHz and 40 MHz that is accurate to within ±5%. Lasing parameters that can be changed, such as output power and pulse repetition rate, are changed by USB communication commands.

Acousto-Optic Tuneable Filter

Using light with a broad wavelength range would not allow control over which pigments, or other protein molecules, would be excited. In order to have selectable excitation wavelength an acousto-optic tuneable filter (AOTF) is used. This device is able to pick out selective wavelengths of light by using the Bragg diffraction principle within an acousto-optic crystal. Bragg's law describes the resulting angle of interacting scattered waves due to incident light on a crystalline structure

UNIVERSITEIT VAN PRETORIA
UNIVERSITY OF PRETORIA
YUNIBESITHI YA PRETORIA

and is given by

$$\sin\theta = \frac{m\lambda}{2d}$$

where θ is the scattering angle, m is the diffraction order, d is the inter-planar distances between the crystal lattice planes, and λ is the wavelength of the incident light. Notice that the angle of scattering is dependent on the wavelength of the light incident on the crystal. This indicates that different wavelengths of light will be diffracted by different amounts. An acousto-optic crystal is defined as a crystal that undergoes a change in optical properties when subjected to vibrational (sound) waves. In terms of an AOTF the mobile compressions and rarefactions due to the sound waves translate into refractive index modulation. This acts as a diffraction grating that extends through a volume, instead of being a planar effect, as a series of periodic refractive index planes and is also known as volume Bragg gratings. In this case the Bragg diffraction depends on the distance between the refractive index planes which is dependent on the wavelength of the sound waves. The equation above can then be rewritten as

$$\sin\theta = \frac{m\lambda_0}{2\Lambda} \tag{2.3}$$

where λ_0 is the central wavelength of the band diffracted and Λ is the acoustic wavelength. By varying the wavelength of the sound waves the angle of diffraction can be controlled. Due to the conservation of momentum in the interaction between the photons and acoustic waves only a small band of wavelengths of light will be diffracted. The wavelength band that will be diffracted can be relatively narrow (in the order of 10s of nanometers) of which the central wavelength is given by

$$\lambda_0 = \frac{\Delta n V}{f} \tag{2.4}$$

where Δn is the birefringence of the crystal. V and f are the velocity and frequency of the acoustic wave, respectively. The intensity of the resulting diffracted light is directly proportional to the amplitude of the acoustic wave. This means that the wavelength, diffraction angle and intensity can be controlled. The setup makes use of a Fianium AOTF with a crystal attuned to the visible spectrum, allowing up to 8 simultaneous wavelengths between 400 nm and >650 nm, each having a bandwidth of approximately 2 nm to 7 nm. It produces a linearly polarised beam and has a maximum diffraction efficiency of $\approx 40\%$. The wavelength bands that are diffracted are implemented through USB communication commands.

Spatial Filter

A uniform Gaussian spatial intensity profile ensures an optimal sample excitation. Due to artefacts in the laser generation and/or AOTF wavelength separation, as well as scattering, the spatial intensity profile of the laser beam might not be uniform. Removing spatial artefacts is, to an extent, achieved by the use of a spatial filter (SF). As mentioned in section 2.1.1 on page 13, a converging light beam does

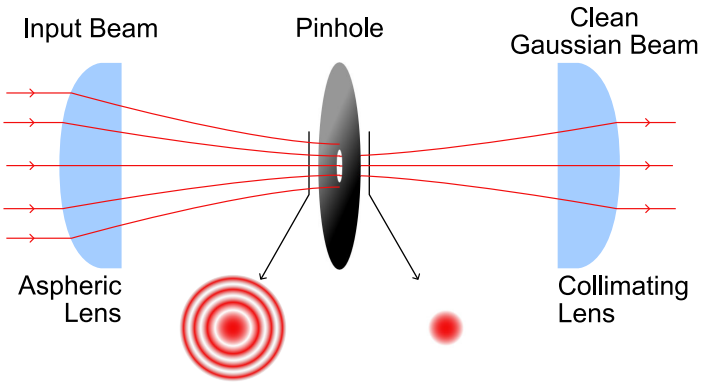

Figure 2.6: Simple diagram of a spatial filter. The beam is focused and the Airy disk passes through the pinhole, while the rest of the beam is blocked. The diverging *cleaned* beam is then collimated. Two insets, as pointed out by the two arrows just before and after the pinhole, indicate how the beam would appear if imaged there.

UNIVERSITEIT VAN PRETORIA
UNIVERSITY OF PRETORIA
YUNIBESITHI YA PRETORIA

not become infinitely small, but instead forms an Airy disk. Focusing a light beam on a pinhole with a radius slightly larger than that of the Airy disk, as defined by eq. (2.1), will effectively *clean* the spatial intensity profile by excluding higher order modes. Refer to fig. 2.6 for a simplified diagram hereof.

Dichroic Beam Splitter

The word dichroic means 'two coloured'. A dichroic mirror is then an optic component that reacts differently to two colours - and in our case two ranges of wavelengths. While reflecting short wavelengths it is transmissive to longer wavelengths. The transition wavelength range - that is the wavelength region where it changes from transmissive to reflective - is small to ensure a decisive cut-off between the two ranges. See fig. B.2 for the transmission spectrum.

Objective

The reflected light is then focused by the objective. The objective used is a Nikon CFI Plan Apochromat Lambda series 100X[1] oil immersion[2] objective that has a transmission of more than 70% between 500 nm and 1000 nm (see fig. B.3) and is housed in a Nikon Eclipse Ti-E/B inverted microscope housing. With a numerical aperture of 1,45 a beam of light with a wavelength of 630 nm will be diffracted to a diffraction limited spot with a radius of ~220 nm.

3D Positioning Stage

The sample is held on a glass cover slip that rests on a Mad City Labs Nano-LPS200 nanopositioning stage. It can move to a 3D position with a 0,4 nm ac-

[1] 100X indicates the magnification factor of the objective.
[2] The oil used has a refractive index of 1.515, as compared to that of 1 for air. Using a medium with a higher refractive index increases the NA that the objective can obtain (see section 2.1.1).

curacy in the X and Y. Instructions are sent to a ND3-USB163 stage controller through USB communication commands which then instructs the stage to move.[3]

Post-Fluorescence, Pre-Detectors

In conventional SMS the sample molecules are immobilised by allowing them to adhere to a surface. Once a satisfactory density of molecule adhesions has been attained (see section 2.1.1 on page 16), a single isolated molecule is placed in the incident excitation light beam and focused on. Partial recapture of the resulting fluoresced light is collimated by the objective and travels via the same path of the excitation beam, but in the opposite direction. The fluorescence then reaches the dichroic mirror and the wavelength band that is longer than the cut-off wavelength[4] is transmitted.

As the excitation laser pulses travel through the components a small amount of light is reflected at each change of medium where there is a difference in refractive index. This is known as back-reflection, and although this effect is weak it must be taken into consideration when using highly sensitive detectors. Only back-reflected light resulting after the dichroic mirror has the chance to reach the detector. In addition, as the dichroic mirror is not perfect, a small percentage of the back-reflected excitation light will be transmitted. In comparison to the low intensity of fluorescence from a single molecule, the intensity of the back-reflected excitation light that gets through the dichroic mirror can typically be at least one order of magnitude larger. To ensure that only fluorescence will be measured a fluorescence filter removes light around the wavelength of the excitation light. A

[3] The stage position is controlled by applying a voltage for each axis. The controller converts the desired position into the corresponding voltage required and applies it.

[4] As mentioned in section 1.1.2 on page 19, the dichroic mirror should be chosen such that the excitation beam wavelength is close to the cut-off wavelength to ensure that most of the fluorescence will be transmitted.

Chroma EM ET665lp fluorescence filter was used that has a cut-off wavelength of 665 nm (see fig. B.2). The light is then focused by the microscopes tube lens onto a confocal pinhole (as discussed in section 1.1.2 on page 19).

Two types of detectors are used for measurements: a CCD camera for spectral measurements and a single photon counter by means of a single photon avalanche diode (SPAD). Working with the sparse fluorescence of a single molecule means making the most of the photons that are available is crucial. To this purpose, if only spectral measurements are needed all the available photons should be directed to the CCD camera. The same holds true for single photon counting measurements where all the fluorescence would be directed toward the SPAD.

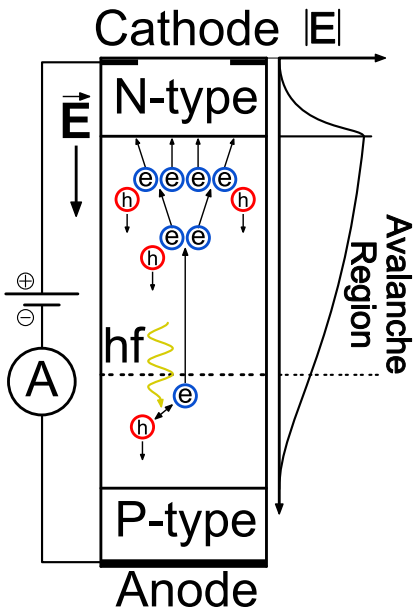

Figure 2.7: A simplistic diagram of a single photon avalanche diode. Photons travelling through the diode have a chance of being absorbed and an electron-hole pair being formed. The resulting electron then moves through the avalanche region and is sufficiently accelerated to cause collision ionisation, triggering an avalanche event and a subsequent spike in the measured current. The region in which this can take place is called the avalanche region. The graph on the righthand side of the diagram is of the electric field strength over the length of the diode.

Notice in fig. 2.5 that directly after the collimating lens there is placed either a beam splitter or a mirror. If both spectral and intensity measurements need to be made simultaneously some portion of the photons should be directed to the one detector and the rest to the other. By using a mirror all the light will be directed to the EMCCD toward for spectral measurement. In reality their exists a third configuration to measure only intensity: neither a mirror filter or a beam splitter. All three desired outcomes can be achieved in this fashion.

UNIVERSITEIT VAN PRETORIA
UNIVERSITY OF PRETORIA
YUNIBESITHI YA PRETORIA

Single Photon Avalanche Diode

Counting single photons is not a trivial task. However, SPADs have successfully been used in SMS measurements [36, 37]. SPADs, are in fact, a special kind of avalanche photo-diode. It consists of a diode which comprises of an electron donating region (n-type) adjacent to an electron accepting (p-type) material.[5] This is known as a p-n junction and has the property that the n-type and p-type interact with each other to form a space charged region. The n-type material loses electrons and becomes positively charged, whereas the p-type material gains electrons and becomes negatively charged, resulting in an electric field (that points from the n-type toward the p-type material). This causes the diode to act as an insulator in one direction, as electrons moving from the n-type to the p-type are decelerated. Applying an electric potential over the p-n junction will either increase or decrease this electric field. With the positive terminal connected to the n-type side and a negative terminal connected to the p-type side the electric field at the p-n junction increases, and the diode is said to be in a reverse bias configuration as it increases the insulating property of the diode. However, increasing the electric potential above some point – called the breakdown voltage (V_b) – causes the insulating property to be overcome.

SPADs operate in a reverse-bias configuration at voltages greater than V_b. The resulting large inherent electric field causes newly generated free electrons on the p-type side to be accelerated toward the n-type side. Most common causes for the formation of new free electrons are thermal generation effects, and photon absorption [38]. When the electric field is large enough the electrons achieve large enough velocities such that collisions with other atoms can cause ionisation

[5] An n-type material is said to have an abundance of free electrons, whereas a p-type material is said to have an abundance of electron holes. It is important to note that these materials remain inherently neutral.

UNIVERSITEIT VAN PRETORIA
UNIVERSITY OF PRETORIA
YUNIBESITHI YA PRETORIA

to occur. Subsequently liberated electrons are also accelerated, and the process can be repeated, causing what is referred to as an avalanche breakdown event. The region in which the electric field is large enough to cause such an event is known as the avalanche region (see fig. 2.7). A sudden rise in free electrons reaching the cathode can typically result in a spike in the current in the order of 100 mA. The leading edge of the current pulse can be detected and time-tagged to supply the arrival time of the avalanche event.[6] Assuming the cause of the avalanche is the absorption of a photon would then mean that single photons could be detected with arrival time information available. To minimise the thermally generated events, and thereby decrease the number of false counts (known as dark counts), the SPAD can be cooled. After an avalanche event, some time is required for the diode to reset and be able to register a subsequent avalanche event. This is known as the dead time and can be as low as the 100 ns regime. The efficiency with which photons are absorbed by a SPAD is dependent on the wavelength.

A Micro Photon Device SPAD is used (PD-050-CTE) that is Peltier cooled and has a dark count rate of 10,5 counts per second. It has a timing resolution of between 77 to 92 ps (FWHM) and has a dead time of 86,1 ns. It has an active sensor area of 50 µm by 50 µm and a peak photon detection efficiency of ~47% at 535 nm. See fig. B.4 for the photon detection efficiency as a function of wavelength. The SPAD is a gated detector, which means that even when supplied with power, the device remains inactive until it receives an external voltage. For this setup the gating voltage is provided by a National Instruments USB-6501 digital I/O device.

[6] The arrival time information supplied by a SPAD is what distinguishes it from a normal avalanche photodiode, where only the rate of photon absorptions can be measured.

Diffraction grating

If spectral measurements need to be made the fluorescence is directed toward a grating to separate the different wavelengths spatially. This is possible thanks to the phenomenon of diffraction. Diffraction is governed by the grating equation:

$$\sin\alpha + \sin\beta_m = \frac{d}{m\lambda} \tag{2.5}$$

where m is the order of diffraction, α is the angle between the incident light and the normal of the grating, β_m is the angle between the diffracted light and the grating normal, d is the groove spacing, and λ is the wavelength of the light. The equation can be written in terms of the commonly used groove frequency which is defined as $G = 1/d$. Different types of gratings exist, each varying in what surface structure is used to diffract light. A blazed (or ruled) grating is one which uses a saw-tooth pattern of ridges, as can been seen in fig. 2.8. The angle between the face of the groove and the plane of the grating is known as the blaze angle, θ_B. By changing this angle the wavelength that has the highest diffraction efficiency[7] can be changed. This means that a ruled grating can be optimised for a particular wavelength of light, providing a significantly high efficiency compared to other types of gratings. As a rule of thumb the wavelength that a grating will be optimised for is given by

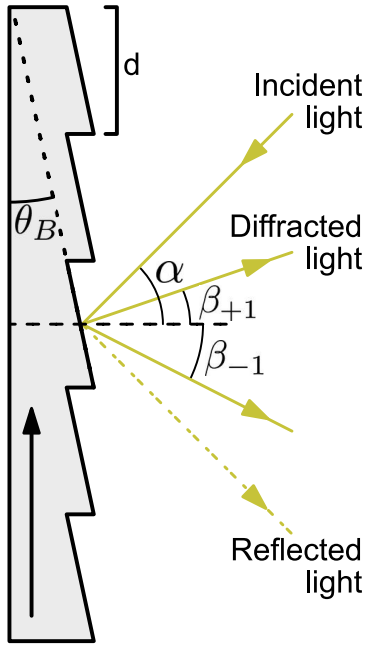

Figure 2.8: Simple diagram of a diffraction grating. The blaze arrow refers to a physical bale arrow on the grating as indication of the direction in which the grating is blazed. Note that the normal shown is with reference to the base.

$$\sin\theta = \frac{m\lambda}{2d} \tag{2.6}$$

[7] Efficiency in this sense pertains to the fraction of energy, for a given λ of the incident light beam, that will be diffracted in the order m.

which is called the blaze condition.

To this end a gold coated Optometrics 3-8880 grating was used with G being 830 grooves per millimetre and θ_B being 19,38° – therefore optimised for 800 nm light – it has a diffraction efficiency of ~70% in the region of 700 nm to 900 nm[8]. See fig. B.5 for the complete diffraction efficiency against wavelength. The grating is 25 mm wide by 25 mm high by 6 mm thick.

Electron Multiplying CCD

The diffracted light is then collimated by a lens and is then directed toward the EMCCD camera. Andor's $iXon_3$ 897 (DU-897E-CS0-EXF) is used as it is remarkably sensitive. This device uses an electron multiplication technology to reach single photon detection capability for each pixel. The sensor consists of 512 by 512 pixels, each pixel being 16 µm by 16 µm, resulting in an active sensor area of 8,4 mm by 8,4 mm. Background noise is reduced by reducing the temperature of the sensor to $-95\,°C$, reaching a dark count[9] of 0,005 events per pixel per second. The efficiency with which photons can be detected by the camera is dependent on the wavelength of the light, as can be seen in fig. B.6.

2.3 Sample Preparation

The journey a single LHCII protein takes from being assembled to ending up at the focal point of an objective in a SMS experiment is impressive, to say the least. After nature takes care of producing and embedding the proteins in the thylakoid

[8] The efficiency with which light is diffracted also depends on the polarisation of the incident light. In this case the efficiency refers to unpolarised light.

[9] Dark count here is defined in the same way as earlier on page 28.

membrane they need to be isolated and prepared for an SMS measurement. A brief discussion of what this involves is given below.

Chloroplasts were isolated from spinach based on a method first used in 1980 [39]. Once isolated the chloroplasts were temporarily subjected to a strong detergent resulting in thylakoid membrane fragments, the majority of which contain PSII which include LHCII. This was first accomplished by ref. [40], and improved upon by ref. [41]. These were used as a guide toward extracting PSII membrane fragments which are called BBY[10] fragments. After the BBYs were successfully isolated they were further broken apart to separate and purify the LHCII complexes as in ref. [42]. As the ratio between ChlA and ChlB in LHCII is fixed and known, measuring the ChlA-ChlB ratio acts as an indicator of the purity of the isolated LHCII. Extinction coefficients used to determine the ratio were as found in ref. [43].

The concentrated purified LHCII complexes were diluted to a concentration of

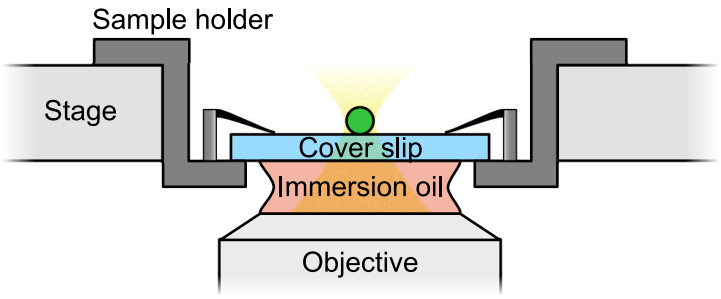

Figure 2.9: Simple diagram of a the sample holder placed on the stage. The samples, diluted in a solution with the desired pH, are immobilised by a poly-L-lysine (PLL) treated coverslip and held in place by a sample holder. The sample holder rests on a stage and is brought into contact with the immersion oil placed on the microscope objective.

[10] Named after the three authors of ref [40].

~10 pM in a solution of 1 mM $MgCl_2$[11], 0,03%[12] n-dodecyl-β,D-maltoside (β-DM) and a pH buffer as determined by the desired pH value. Glass coverslips were first cleaned by submersion in ethanol while being sonicated for five minutes. A treatment of PLL was achieved in a similar manner by using 10% deionised water dilution. The excess PLL solution was washed off by a last sonication step in only deionised water. By applying approxiamtely 1 µL of the LHCII solution to a dried PLL coated glass coverslip a monolayer of LHCII complexes binds to the surface at a density of ~10 complexes per 10×10 µm^2. The resulting measurement setup is illustrated in fig. 2.9.

Non-photochemical quenching can be emulated to varying extents (see chapter 4 on page 46) by choosing a range of different solution pH values. pH values of 8, 7, 6, 5 and 4 were used, by using buffers as shown below.

ph 8 20 mM tris(hydroxymethyl)aminomethane (Tris) with an effective buffer range of 7,5 - 9,0.

pH 7 20 mM 4-(2-hydroxyethyl)-1-piperazineethanesulfonic acid (HEPES) with an effective buffer range of 6,8 - 8,2.

pH 6-5 20 mM 2-(N-morpholino)ethanesulfonic acid (MES) which has an effective buffer range of 5,5.

pH 4 15 mM sodium citrate and 25 mM HEPES[13].

[11] The $MgCl_2$ aids the adhesion of LHCII to the poly-L-lysine (PLL) layer

[12] This is called mass concentration and is defined by m/V where m is the mass of the constituent in question and V is the volume of the solution (not the solvent).

[13] Sodium citrate is usually used in concert with citric acid – of which the ratio of the concentrations determine the effective buffering pH value – which was not used, however, the pH after the measurement was tested and was found to have remained constant.

UNIVERSITEIT VAN PRETORIA
UNIVERSITY OF PRETORIA
YUNIBESITHI YA PRETORIA

Chapter 3

Software Development

In the same way a musical conductor integrates individual contributions in a constructive manner to form an orchestra, different hardware components need to be orchestrated to work together in order to successfully perform a measurement. Expanding the analogy, just as a spectator would find it difficult to truly understand the workings of the conductor without some prior expertise in the field, it would require a considerable effort for a user to work through the programmatic code and gain insight in how the software works that controls the measurement process of the SMS setup. This section is an attempt to equip the reader with a basic insight into the software that has been developed up until the publication of this dissertation.

3.1 Hardware-Software Interfacing

In choosing which programming platform to use for the setup one should consider the requirements that need to be met. One obvious requirement is that the platform needs to be able to interface with hardware. Additionally, when taking into account that some processes need to take place in parallel, we realise that said platform should be able to allow for parallel computing. Many experimental systems that share these requirements have made use of a graphical programming platform developed by National Instruments (NI) called LabVIEW™. The graphical nature of LabVIEW™ is both a disadvantage and a boon. For those well versed in text-based programming the graphical environment demands a paradigm shift to be made as LabVIEW™ contains almost no text-based commands and uses a data flow execution strategy. Those that approach it afresh find it intuitively understandable. For an introduction to the basics of LabVIEW™ see this[1] website. It is highly advisable for those that need to involve themselves greatly in the LabVIEW™ code to attempt to obtain the Certified LabVIEW Associates Developer (CLAD) certificate.[2] At the time of publication LabVIEW™ 2013f2 32 bit was being used.

Before any discussion is made about the code itself, however, it is crucial to inspect the manner in which the physical devices involved in the measurement interface with the software. Toward this goal fig. 3.1 more or less encapsulates all the necessary information.

As mentioned earlier, the laser communicates with LabVIEW through a USB

[1] `http://www.ni.com/getting-started/labview-basics/`

[2] This is done by completing NI's Core 1 and Core 2 courses. See NI's homepage for more information.

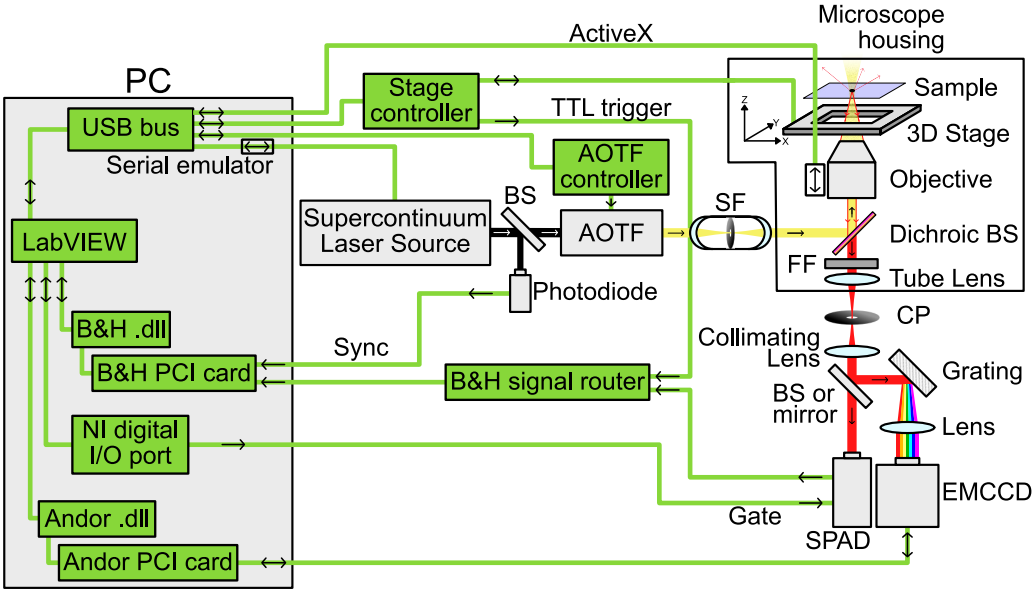

Figure 3.1: An illustration of the manner in which the hardware components interface with LabVIEW™. The green line represents communication channels and the arrow the direction of the communication. In the case of two-way communication a double arrowed line is used. The grey box on the left indicates which features are incorporated into the PC.

driven serial communication emulator. This means that the laser sends and receives ASCII text commands via a USB connection, but interprets it as serial communication. A serial emulator is used to allow the USB connection to be used as if it were a serial port. LabVIEW can interface directly to the emulated serial port. All of the configurable settings of the laser can be determined by these text based commands. As an example, the current repetition rate of the laser can be requested by sending the text command `R?`, to which the reply would be `R=20.0`, indicating a rate of 20 MHz.

The 3D positioning stage is controlled by a stage controller, which in turn communicates through USB with LabVIEW™. Although not shown in fig. 3.1 Mad City Labs have provided a LabVIEW™ compatible dynamic-link library (DLL) through which the communication between LabVIEW™ and the stage controller are made possible. DLLs in this scenario can be seen as a file that contains

UNIVERSITEIT VAN PRETORIA
UNIVERSITY OF PRETORIA
YUNIBESITHI YA PRETORIA

functions that can be called to perform tasks that would otherwise have required a fundamental knowledge of the instrument it interfaces with. This allows us to send commands within the LabVIEW™ environment to hardware without knowing exactly how those commands are realised. Apart from the output the controller sends to the stage, a transistor-transistor logic (TTL) trigger signal can be sent to the Becker & Hickl router, which will be discussed soon. Suffice it to say this is used to eventually provide time information to LabVIEW™.

The AOTF also follows this pattern, except that the suppliers provided an additional stand alone LabVIEW™ generated executable. This is to say that AOTF communication has, as of yet, not been incorporated directly into the LabVIEW™ environment, as the stand alone software has been sufficient. This would at some stage in the future have to be changed, to allow programmatically generated changes to the wavelength of the excitation light.

The Nikon microscope housing's objective stage can also be controlled by ActiveX controls through USB. An ActiveX control is a collection of commands that can be accessed by many application programs, such as LabVIEW™. In this sense it is similar to DLLs. This allows LabVIEW™ to programatically change the distance between the objective and the sample, thereby changing the focus.

As the SPAD only generates pulses for each detected photon, an additional device needs to capture the inferred time information. A Becker & Hickl (BH) SPC-130-EM PCI card module and a BH 8 channel HRT-82 TCSPC[3] routing unit is used. The router identifies which channel received a pulse and sends the pulse and the channel information through to the SPC module. As mentioned in section 2.1.3, TCSPC measurements include both the absolute arrival time (that is the time since the start of the measurement) as well as the laser pulse relative time (that is the

[3] See section 2.1.3 on page 20.

UNIVERSITEIT VAN PRETORIA
UNIVERSITY OF PRETORIA
YUNIBESITHI YA PRETORIA

time since the latest laser pulse). In order to measure a relative time, timing information of the laser pulse needs to be available to the SPC module. To this end, a photodiode circuitry that generates a TTL pulse for each laser pulse was built and included in the setup as indicated in fig. 3.1. This signal - called the sync signal - is sent directly into the SPC module. The procurement of a LabVIEW™ compatible DLL from BH allows communication between the SPC module and LabVIEW™.

A somewhat unintended use of the SPC module is that we were able to trick the module into accepting a TTL signal from the 3D stage controller as if it were a photon. This means that each time the stage would arrive at the next position during a predefined sequence of positions the SPC module would detect a *quasi-photon*. Using the absolute arrival times of the *quasi-photons* from the stage a correlation between the position of the stage and the intensity of the fluoresced photons can be computed. This is to say that we know where the stage is for any given fluoresced photon. This is particularly useful when building an intensity map for a given area as mapped out by the stage (see section 3.2 on page 39). Lastly, an NI digital I/O device used to gate the SPAD and is controlled directly through LabVIEW™ by USB.

The EMCCD follows a similar communication channel to that of the SPC module, in that the detector interfaces to a PCI card inserted into the PC, which in turn uses a LabVIEW™ compatible DLL (provided by Andor) to interface with LabVIEW™.

3.2 LabVIEW™ Code

The overall architecture of the code is one that relies on user cues via the graphical user interface (GUI) before performing most tasks, while some tasks continually take place in the background. So-called *state machines*[4] are programmatic structures that are perfectly suited to this type of software design. In this structure the program is compartmentalised into different states which the state machine switches between. Figure 3.2 illustrates how the state machine concept was implemented for this setup. Note that only a selection of important states have been included in this diagram.

As certain actions must be taken at the very start of the program the state machine enters an initialisation state initially by default. This state is followed by a state that loads the previous settings. The state machine then enters a state in which it

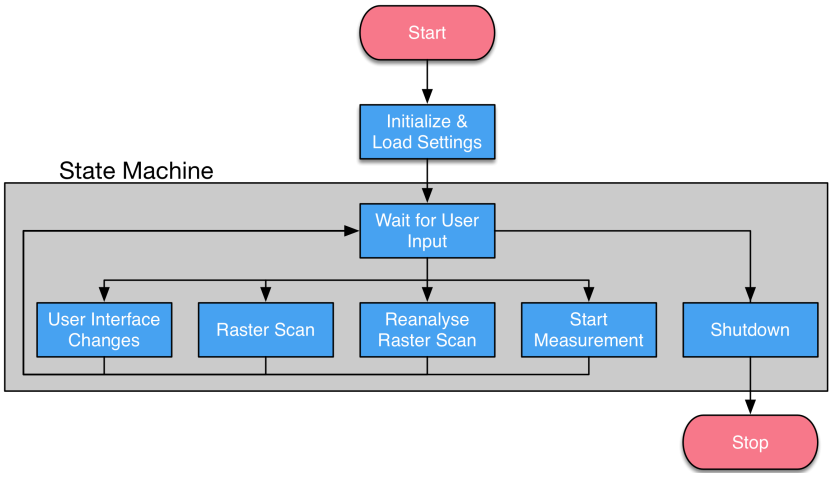

Figure 3.2: A flow diagram of the overall state machine of the code to depict the underlying programmatic algorithm. The start and stop of an algorithm are depicted by a red circular rectangle. Blue rectangles represent processes or functions that are executed.

[4] For a tutorial on state machines by NI see `http://www.ni.com/tutorial/7595/en/`

Figure 3.3: A simplified flow diagram of the raster scan process.

waits for user input. The next state is determined by what user input is supplied. Suppose the user changes something that requires a change or update of the GUI. A *UI Changes* state is entered, the GUI elements that need to change are identified and updated, and the state machine is directed back to the *Wait for user input* state.

A complete and protracted walkthrough of the code is unrealistic. Conveniently one process makes use of most of the vital processes. Consequently, the discussion of the procedure below will cover most of the important aspects.

A raster scan (RS) is a process that attempts to ascertain the positions of fluorescing particles within a user defined area. Intensity measurements at points in the designated area build up an intensity map. Image analysis functions fix the positions of particles that meet the required criteria. Proximity to other particles or the edges of the scanned area, expected intensity magnitude and particles size are all factors that are used to decide whether or not the positions are to be used or discarded. As seen in fig. 3.3 the RS process can be compartmentalised into three parts: acquisition, extraction and analysis. Each of these will be expanded upon.

3.2.1 Acquisition

As the data acquisition of a RS makes use of the stage to perform and record the position movements, as well as the detection of fluoresced photons, two processes need to take place in parallel. BH's SPC-130-EM module provides different types of measurement options. The best suited for this application makes use of buffer memory situated on the PCI card.

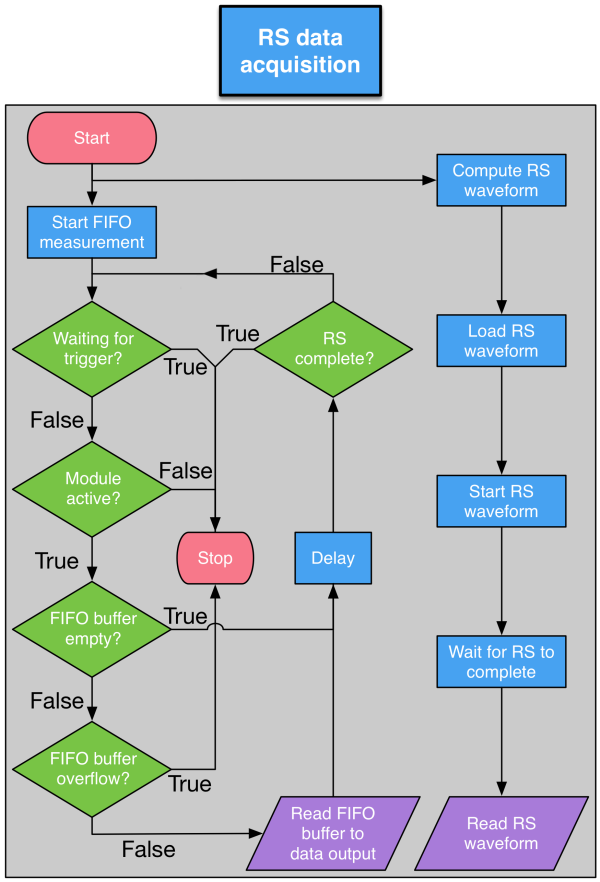

Figure 3.4: A simplified flow diagram of the raster scan acquisition process. Green diamond shapes indicate points in which crucial decisions are made Parallelogram with a purple fill are used to indicate important data storage.

When a photon is detected its arrival time information, as well the router channel it was received from, are saved in binary format to the buffer. The buffer works on a first-in first-out (FIFO) basis. Consider three photons, the first called A, the second B and the last C. FIFO buffering would mean that A is added, then B and lastly C. The first element that would be read from the buffer would be A; it was first in, and first out. The second available element would then be B, and the last C. As buffers have a fixed storage capacity, when the buffer is full the information that would have been stored is lost. When this happens the buffer is said to have overflowed. To prevent an overflow from occurring the buffer needs to be read out at a rate faster than it is written to. However, as a large portion – possibly the entire – buffer can be read out in a single reading it is not difficult to prevent an overflow by having using a realistice readout rate.

As seen in fig. 3.4, the first step in the acquisition process is to start the FIFO measurement. Then follows a loop that reads the FIFO buffer at a constant rate. It first checks whether or not the SPC module is waiting for a trigger. Absence of

UNIVERSITEIT VAN PRETORIA
UNIVERSITY OF PRETORIA
YUNIBESITHI YA PRETORIA

a waiting trigger state means that the measurement has not started, or that it has stopped for some reason and the process terminates with an error. Alternatively, it reads the active state of the module. This is an internal check. The buffer is then checked to see if data is available to be read. If no photons have been detected the reading steps are skipped. Conversely, if photons have been detected the buffer is then checked for an overflow event. If an overflow did occur the process ends after generating an error message. If no error has occurred the read out and the data are stored. A delay ensues with a duration that assures a roughly constant loop rate. If the parallel process that directs the RS movement has not yet been completed the loop reiterates.

As mentioned, the second part of the acquisition process controls stage movement. The first step is to compute the desired sequence of positions the stage should move to, as well as what duration the stage should spend at each position. Collectively these instructions are referred to as a waveform. The waveform is then sent to the stage controller and started. The stage executes the waveform as follows: the stage is told to move to the next position, the true position is read, and after the set delay the process is repeated. As soon as the waveform has been completed the true positions are read and stored.

3.2.2 Extraction

To understand why an extraction process is needed and how it works it is necessary to examine in what manner the SPC module stores the photon information. Figure 3.5 should be used as an aid in understanding how photons are extracted from the FIFO data buffer. Each photon data segment consists of a *frame*, which in turn comprises two *words*.[5] As the first word is added to the frame first, fol-

[5] In computer architecture terms a *word* is a 16 bit binary unit.

lowed by the second, the order of the words in the frame is reversed, containing first what is called Word 1, and then Word 0.

To circumvent this potentially confusing situation the two types of words are separated into their own arrays, as illustrated in fig. 3.5c.

Of the 32 bits[6] used to store one photon's information, 12 bits are dedicated to storing, what is referred to as, a macro arrival time. The largest value that 12 bits[7] can represent is 4095*. This value indicates how many times an internal macro clock has ticked before registering the photon. Therefore, the macro time is the stored value multiplied by the duration of the one tick. In our case the macro clock is 25 ns, which in turn means that the largest macro time that can be stored for each photon is 102,375 µs. Obviously, this raises the question of

Photon Frame Binary Breakdown

a)

		bit 7	bit 6	bit 5	bit 4	bit 3	bit 2	bit 1	bit 0
Word 0	byte 0	MT:7	MT:6	MT:5	MT:4	MT:3	MT:2	MT:1	MT:0
	byte 1	R:3	R:2	R:1	R:0	MT:11	MT:10	MT:9	MT:8
Word 1	byte 0	ADC:7	ADC:6	ADC:5	ADC:4	ADC:3	ADC:2	ADC:1	ADC:0
	byte 1	Invalid	MT OV	GAP		ADC:11	ADC:10	ADC:9	ADC:8

Overflow Frame Binary Breakdown

b)

		bit 7	bit 6	bit 5	bit 4	bit 3	bit 2	bit 1	bit 0
Word 0	byte 0	Cnt:7	Cnt:6	Cnt:5	Cnt:4	Cnt:3	Cnt:2	Cnt:1	Cnt:0
	byte 1	Cnt:15	Cnt:14	Cnt:13	Cnt:12	Cnt:11	Cnt:10	Cnt:9	Cnt:8
Word 1	byte 0	Cnt:23	Cnt:22	Cnt:21	Cnt:20	Cnt:19	Cnt:18	Cnt:17	Cnt:16
	byte 1	1	1			Cnt:27	Cnt:26	Cnt:25	Cnt:24

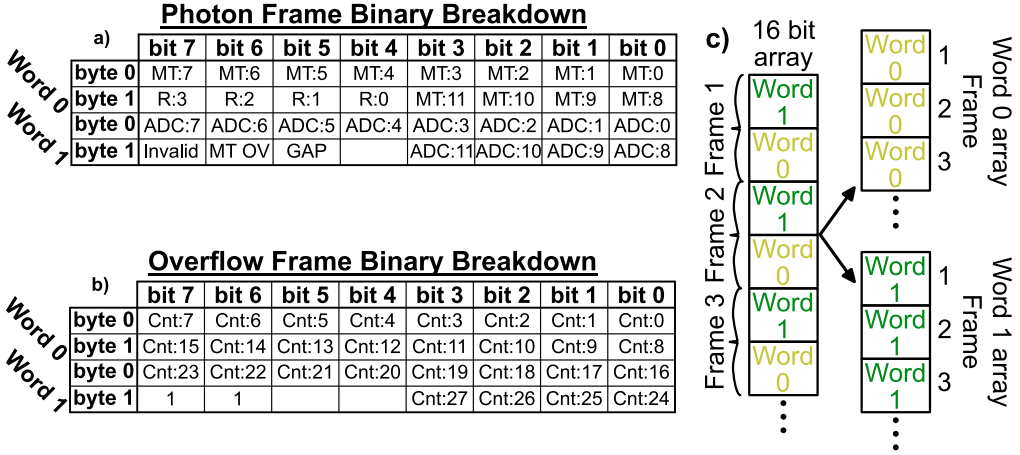

Figure 3.5: Information needed to extract photon information from FIFO data buffer. Table **a)** and **b)** are breakdowns of bit positions for variables stored in photon and overflow frames respectfully. Note: the bytes are saved in big-endian, which is to say that the most significant bit is stored first (at the lowest storage address). Illustration **c)** serves to indicate the order in which frames occur within the FIFO buffer.

[6] 2 words × 16 bits = 32 bits

[7] Assuming only positive numbers.

* This is given by $2^m - 1$ where m is the number of bits available.

how longer times are measured. BH's solution was to define two types of frames, the first being a frame containing photon information, as mentioned above, while the second is a frame dedicated to give a counter of how many macro time overflows have occurred. Let's say, for example, that between two photons a period of 10 ms passes, in which case the macro time would have overflowed 97 times. Before the newest photon frame is stored in the buffer, the SPC module first stores an overflow counter frame. This frame contains a 28 bit counter, which in this case would store a value of 97, allowing the accumulated macro time – the absolute time – to be calculated.

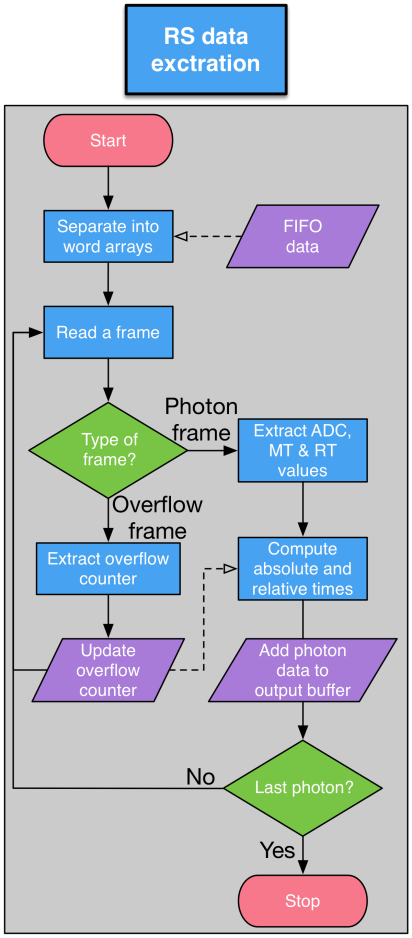

Figure 3.6: A flow diagram of the raster scan extraction process. Dashed lines with a hollow arrow point that point away from a parallelogram indicate that the stored data being is being used by the indicated process.

The photon frame also includes a 12 bit value called the ADC value (analog to digital converter), a 4 bit value representing the router channel the photon was detected through, and three flags[9]. The *Invalid* flag indicates whether or not the photon is invalid. A value of 0 says that it is valid. The macro time overflow (*MT OV*) flag would be 1 if a macro time overflow had occurred before the photon in question had been detected. The *GAP* flag would be 1 if there exists a chance that the FIFO buffer had overflown, causing a loss of photons before the photon in question was written to the buffer.

[9] A flag is a single binary value that acts as a boolean value to indicate certain properties.

With all of this known, we can now mathematically define the following. The laser pulse relative arrival time, or micro time T_{micro}, is given by

$$T_{micro} = \frac{(4095 - ADC)TAC_{range}}{4096TAC_{gain}} \tag{3.1}$$

where ADC is the micro time counter, TAC_{range} is a value that indicates the largest measurable micro time, and TAC_{gain} is a value that is used to indicate by what factor the range of the micro time has been reduced to gain an increase in temporal resolution. TAC_{range} and TAC_{gain} are values that are set during the initialisation of the SPC module and the measurement preparation, and should therefore be known. The macro time – i.e. the time used to keep track of the absolute time – is given by

$$T_{macro} = T_{macro\ clock}\, MT \tag{3.2}$$

where MT is the micro time counter and $T_{macro\ clock}$ is the macro clock duration. The macro overflow time is given by

$$T_{OF} = 4095\ T_{macro\ clock}\ OF \tag{3.3}$$

where OF is the macro overflow counter. Using eqs. (3.1) to (3.3) we can define the absolute time, were the N^{th} stored photons absolute time is given by

$$\begin{aligned} T_{abs_{N+1}} &= T_{abs_N} + dT_N \\ &= T_{abs_N} + T_{micro_N} + T_{macro_N} + T_{OF_N}. \end{aligned} \tag{3.4}$$

See figs. C.1c and C.1d for the LabVIEW™ code of this process. Note that if there was no overflow frame before photon frame $N = 1$, T_{OF_N} can be said to be zero. The unit of all time values is in tenths of nanoseconds (0,1 ns).

A frame is indicated to be an overflow frame when both the *Invalid* and the *MT OF* flags are true (that is that they have a value of 1, as seen in fig. 3.5b). For a tabular breakdown of the binary values for the photon frame and the overflow frame, see fig. 3.5a and fig. 3.5b, respectfully. Figure 3.6 has been expanded upon in fig. C.1.

3.2.3 Analysis

The last step of the RS process is one of consolidation; the photon information translates into pixel intensities via a process illustrated by fig. 3.7. When the absolute times of two consecutive positions are known the number of photons that were detected between the two can be counted. This is done for all the positions in the waveform. The result is a two dimensional intensity mesh. To account for the discrepancies between the desired and measured positions a two dimensional interpolation algorithm is applied as provided by LabVIEW™. The result is then converted to an image and subjected to an image analysis routine that identifies the central positions of particles that meet the criteria as mentioned in section 3.2 on page 39.

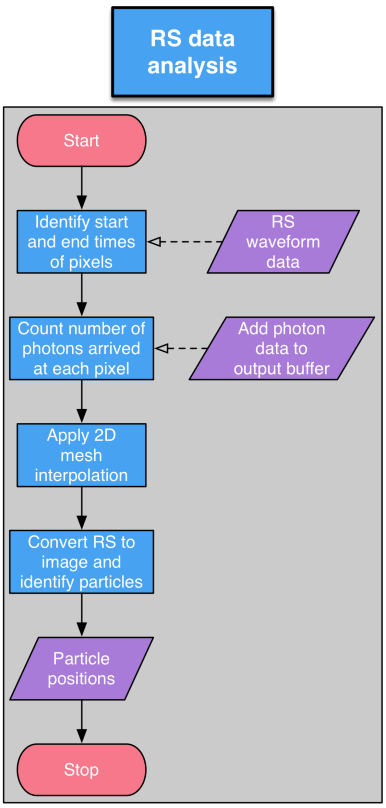

Figure 3.7: A flow diagram of the raster scan analysis process.

UNIVERSITEIT VAN PRETORIA
UNIVERSITY OF PRETORIA
YUNIBESITHI YA PRETORIA

Chapter 4

Data and Results

The increase in pH gradient over the membrane has been shown to be the trigger of NPQ [44]. Furthermore, it has been shown that qE in isolated LHCII complexes can be emulated by lowering the environment pH [45, 46]. This means the quenching introduced into LHCII by qE can be investigated by performing a pH dependent study.

It is important to understand that each detected photon represents an excitation-fluorescence event of a system in a functional state. When considering fluorescence intermittency these states are either the bright state, the dim state or some intermediate state. Unfortunately, only detecting photons does not intrinsically indicate in which of these states the system was in at the moment of fluorescence. These states, therefore, need to be resolved from the fluorescence intensity measurement, which is obtained by counting the number of photons detected in a chosen time bin (similar to RS intensity, see section 3.2.3 on page 45). However, due to the quantised nature of light, the temporal resolution is limited by Poisson-distributed noise – also known as shot noise. The extent with which this noise

UNIVERSITEIT VAN PRETORIA
UNIVERSITY OF PRETORIA
YUNIBESITHI YA PRETORIA

obscures the fluorescence intensity level is proportional to the square root of the number of photons that are detected within the bin. A statistical method used to resolve the start of new intensity levels is described in [47]. In short, a predetermined factor of the standard deviation of the shot noise is used to determine what the probability is that a new intensity bin belongs to the same intensity level or not. Even more, the method considers multiple consecutive points. For example, the probability that four consecutive intensity points that each differ from the average of the current intensity level by one standard deviation belong to a new intensity level is 99.937% The result of a few analysed fluorescence intensity traces can be seen in fig. 4.1.

4.1 Fluorescence Categorisation Study

In order to gain some perspective on how emulated NPQ alters the system, a categorisation of different behaviours that were identified were tracked with the change of pH. Figure 4.1a shows the binary switching behaviour as mentioned in section 1.3 on page 10, and this is considered **normal** binary switching behaviour. Published work has only investigated the *on/off* behaviour [23, 27, 47–49]. However, as previously mentioned, the systems occasionally deviate from this usual two-level blinking behaviour and access intermediate intensity levels as seen in fig. 4.1c and fig. 4.1d. In some cases the system returns to binary switching – this will be referred to as **reversible intermediate** traces – and in some cases not, then called **irreversible intermediate** traces.

Attempting to categorise blinking behaviour has, as of yet, not been done before. This study included approximately one hundred traces for each pH value dataset. Each category is defined by behaviour that can be noted through visual inspection.

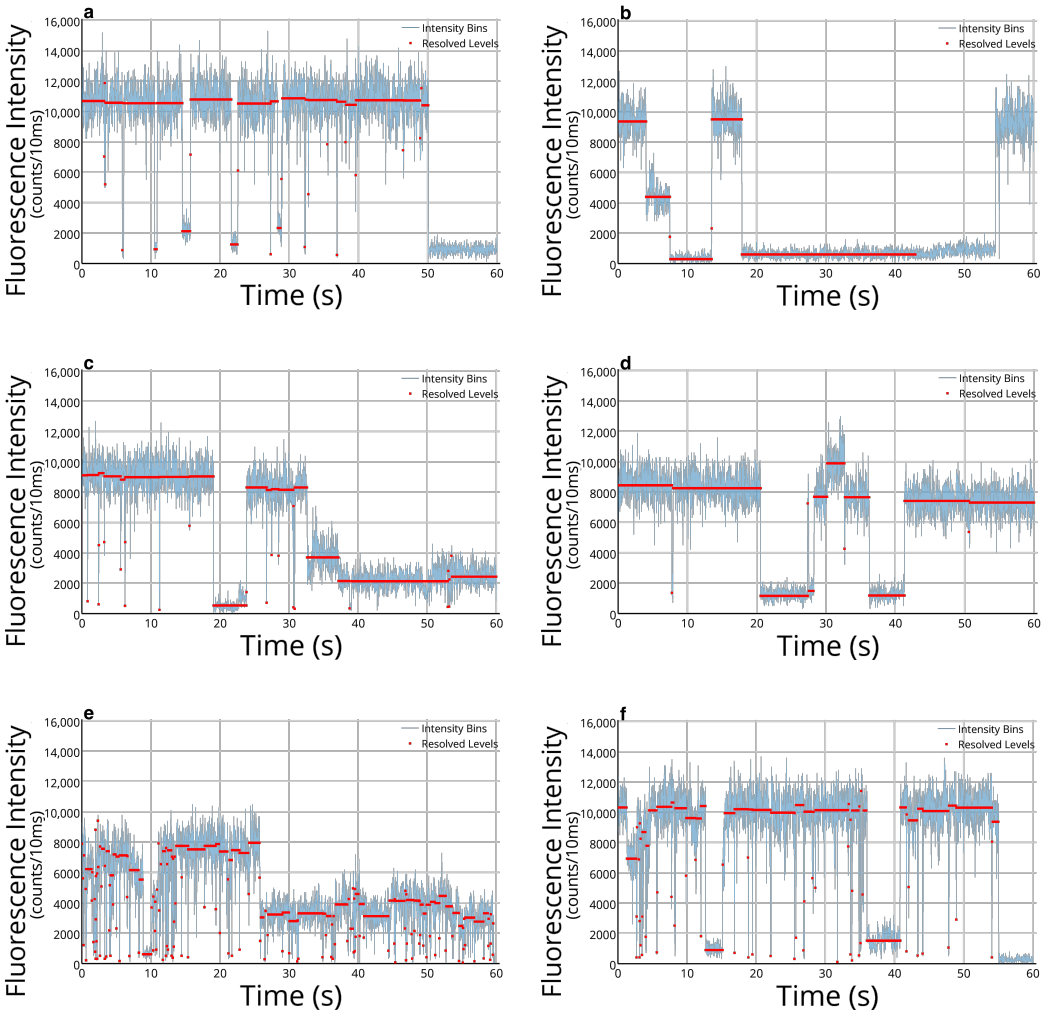

Figure 4.1: Examples of fluorescence intensity traces, all of which were measured without emulating NPQ (that is at pH 8) for a duration of sixty seconds. An example of normal fluorescence behaviour is given in **a)**. In **b)** is given an example of a seemingly dead trace. In **c)** and **d)** are examples of irreversibly and reversibly accessed intermediate states. The latter starts in an intermediate state and briefly returns to the normal bright state. Lastly, **e)** and **f)** are examples of traces exhibiting high jumping frequency as well as accessed intermediate state reversibly and irreversibly. The fluoresced detected photons were binned in 10 ms bins. It should be noted that, whereas internal protein mechanics could alter the fluorescence intensity, the absolute maximum intensity between traces could differ due to some experimental effects such as imperfect focusing. Intensity levels are resolved by statistical analysis, as discussed above.

UNIVERSITEIT VAN PRETORIA
UNIVERSITY OF PRETORIA
YUNIBESITHI YA PRETORIA

The definition of the three categories allows only for boolean values in that there are no degrees of freedom in assigning a trace to belong to one of these categories. This means that no observable error exists for the above-mentioned categories.

In addition to those mentioned above another type of behaviour can be noted. The rate that the system 'jumps' from one state to another is known as the switching rate. A number of complexes seemed to have a distinctively high switching rate, as can be seen in fig. 4.1e and fig. 4.1f. Further investigation hereof leads to formation of another category: **high switching frequency** behaviour.[1]

To avoid including measurements that do not represent 'healthy' systems – that is complexes that have undergone photobleaching or protein denaturation[2] – the algorithm attempts to identify 'dead' complexes. Surprisingly, some complexes were found that remained in a dim state for long times only to return to another state after several seconds. This observation eludes to an intrinsic problem in attempting a thorough categorisation of fluorescence behaviour, in that categorical manifestations could be present in the system without having been measured during the experiment.

Inspection of fig. 4.2a reveals that the fraction of **normal** traces remains more or less constant as NPQ is emulated to higher degrees. The same is mostly true for the traces that accessed intermediate intensity levels **reversibly** except that the largest fraction of these were found at pH 9. Interestingly, the **irreversible** fraction increases dramatically in comparison to the reversible. A decrease is seen in the fraction of **high switching frequency** traces with the escalation of the mimicked

[1] At the time of this work the distinction between normal and high switching rates was done by means of a quasi-subjective inspection. For some datasets two populations were not successfully identified and the subsequent categorisation was done by inspection only. In future work a robust statistical methodology will be developed and employed.

[2] Denaturation is when a protein undergoes structural degradation by unfolding.

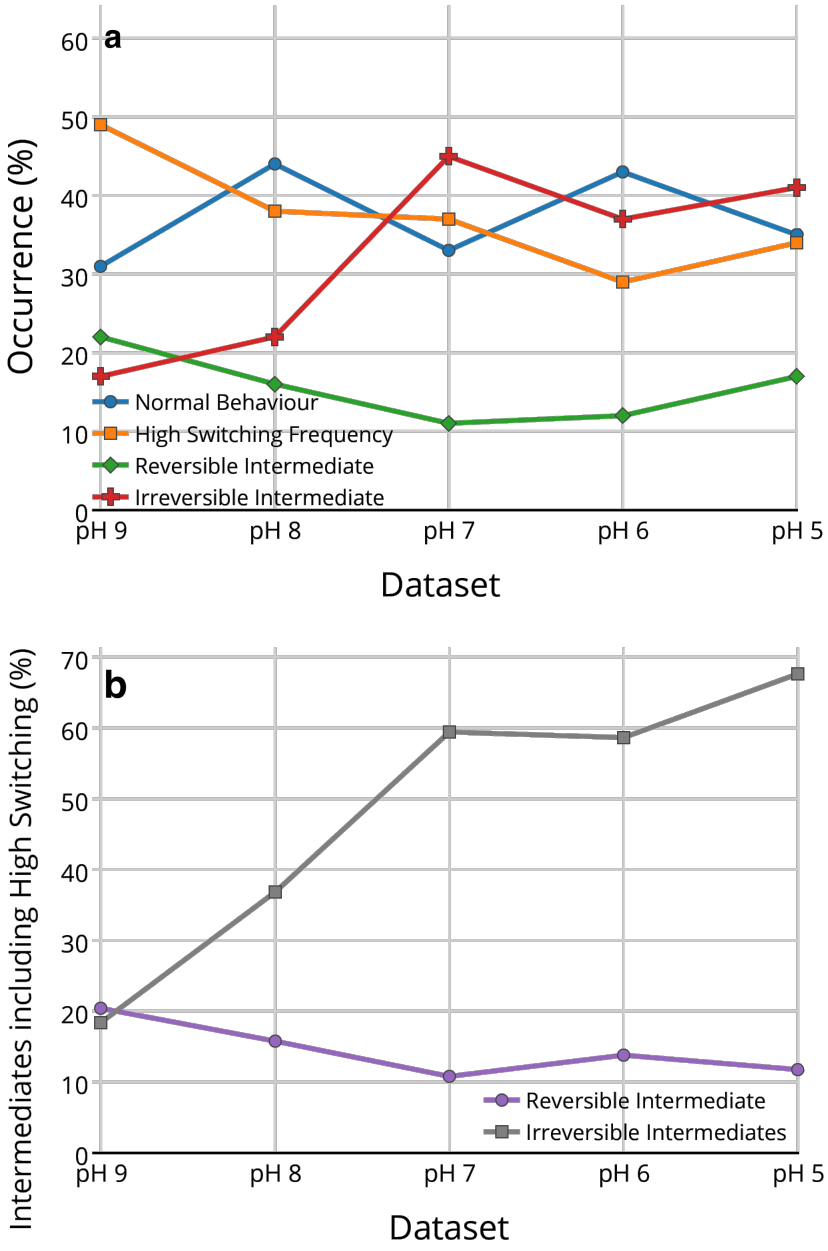

Figure 4.2: Comparing fluorescence intensity trace categorisation of **a)** the main categories, and of **b)** high jumping frequency behaviour that also accessed intermediate states both reversibly and irreversibly. Values are shown as percentages of datasets for each pH value, where the datasets contain approximately one hundred complexes. Some of the categories are not mutually exclusive and therefore all percentage values in the datasets should not be expected to summate to unity. It is important to note that the **reversible** and **irreversible** category traces could also contribute to the **high switching frequency** category, whereas the **normal** category excludes all other categories. As pH 4 is not a natural state for LHCII these values should not be considered when analysing the results.

NPQ.

A possible relationship between the switching rate and the intermediate states was also found, as illustrated in fig. 4.2b. More specifically, the fraction of **high switching frequency** traces that entered **irreversible** intermediate states grew considerably as NPQ was increased. However, the fraction that entered **reversible** intermediate states in concert with high switching frequencies decreased somewhat as NPQ was increased.

4.2 Fluorescence Lifetime vs Intensity Study

As mentioned in section 1.3 on page 10, measuring the fluorescence lifetime of the system is a direct measurement of the extent to which the system is quenched. For this reason measuring the lifetime is an invaluable tool when studying NPQ in LHCII.

Figure 4.3 reveals a mostly linear relationship between fluorescence intensity and lifetime. This directly follows from the rate equation (refer to section 1.3) which implies that the excitation quenching due to NPQ is a process that competes with the other processes at the site of fluorescence emission. This is to say that after the excitation relaxes to the most stable (lowest energy) site – called the terminal emitter – quenching would not only prevent fluorescence, resulting in a drop of fluorescence intensity, but would also cause the excitation lifetime[3] to decrease, as illustrated in fig. 4.4a. This has been shown before in [50, 51].

In addition to the linear relationship, a non-linear population is observed. This deviation also increases as NPQ is emulated more extensively; this is best seen

[3] This is defined as the duration after which, on average, $1/e$ of the excitations are de-excited.

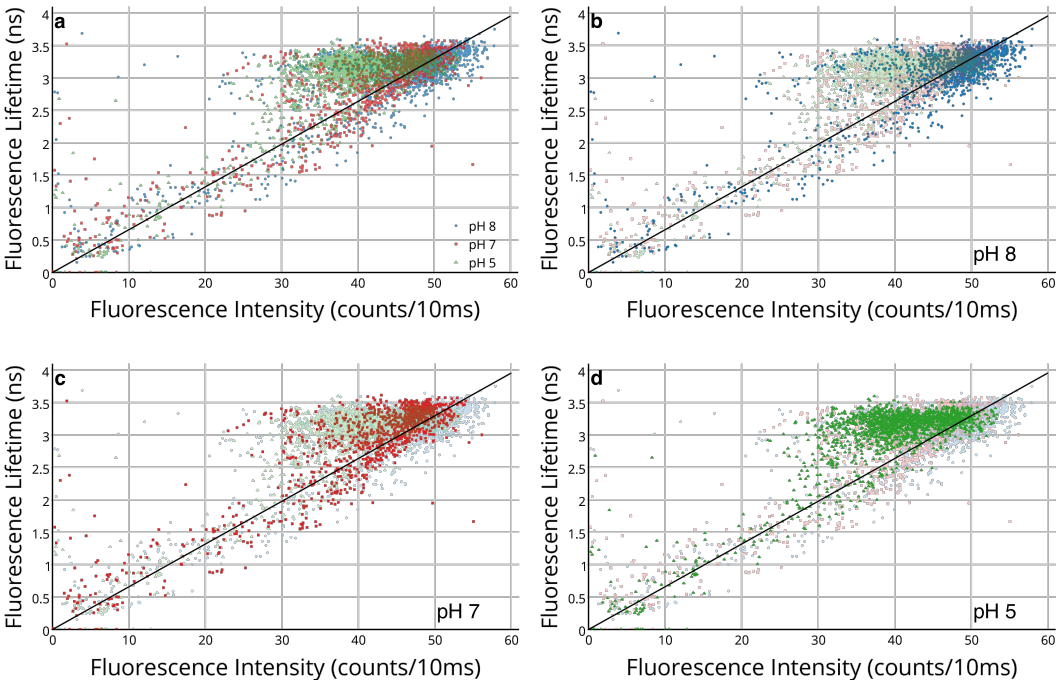

Figure 4.3: Fluorescence lifetime vs intensity study of **a)** datasets pH 8, pH 7 and pH 5 overlaid. For a clearer distinction of what changed **b)**, **c)** and **d)** show pH 8, 7 and 5 highlighted. Each datapoint represents the intensity and lifetime of a single resolved level. Each dataset comprises more than one hundred traces, each trace containing in the order of tens to hundreds of resolved levels. The lifetimes where determined by applying Gaussian exponential decay fitting of the excitation relative photon arrival time histogram data. The high intensity and long lifetime data point correspond to the *bright/on* state. As the accompanying *dim/off* state is defined by its lack of photons and therefore these data points are sparse in comparison. The middle population represents the intermediate levels.

when comparing fig. 4.3b (pH 8) to fig. 4.3c (pH 7), to fig. 4.3d (pH 5). Two possible explanations for this behaviour will be discussed here.

The first possibility is that – as the extent of NPQ emulation increases – the quenching is more likely to take place before the excitation relaxes to the terminal emitter. If this takes place the excitation would not be emitted as a photon, causing a decrease in fluorescence intensity. However, if the excitation reaches the terminal emitter, quenching would no longer be a competing process to the other possible processes, and the lifetime would remain unchanged. This absolute

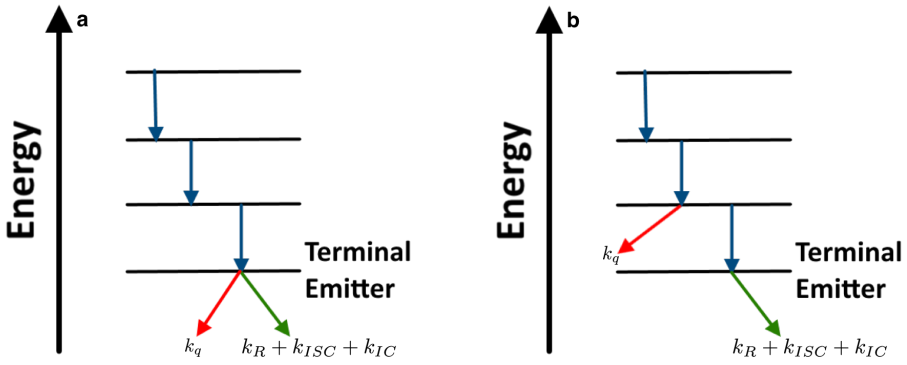

Figure 4.4: Illustrations for two cases of energy evolution within LHCII after absorption of a photon. The first being the **a)** competing and the second the **b)** non-competing quenching as explanation for linear and non-linear population in fluorescence lifetime versus intensity study.

decrease of fluorescence intensity would then deviate from the linear tendency. Such an explanation was offered in Ref. [51]. The other possibility is that the protein undergoes structural changes due to the decrease in pH that results in the loss of peripheral pigments. Fewer pigments would result in a decrease of absorption cross-section, resulting in fewer photons being absorbed, which in turn would mean fewer excitations would be present in the system, and finally that the rate at which photons are fluoresced by the system would decrease. To allude to which of the two possible mechanisms (if any) is most likely the cause of the non-linear population the study can be redone with the key difference being that the pH environment is changed during a single run from pH 8, to pH 5, and back to pH 8*. If the return to pH 8 is accompanied by the same degree of non-linear population as the initial pH 8 state it would suggest that the non-linear population is caused by a reversible process which is caused by the emulation of NPQ, and not by a structural change, as would be the case for pigment loss.

* It would be necessary to exclude pH 4 as it has been shown that LHCII definitely undergoes pigment loss due to slight denaturation at this pH.

UNIVERSITEIT VAN PRETORIA
UNIVERSITY OF PRETORIA
YUNIBESITHI YA PRETORIA

Chapter 5

Synopsis

This dissertation had several objectives.

Chapter 1: to prepare the reader with the necessary theoretical knowledge to understand the result of the study, but almost just as important, to place the results in context.

Chapter 2: to equip the reader with a basic understanding of how single molecule spectroscopy is achieved, as well as to act as a practical guide to the experimental setup built at the University of Pretoria, South Africa.

Chapter 3: to briefly record – and discuss – some of the crucial programmatic concepts that was developed in-house, and to aid the reader in delving into the code themselves.

Chapter 4: to present the results acquired and draw all possible conclusion therefrom.

Assembling the setup and coding the software was what most of my time was

UNIVERSITEIT VAN PRETORIA
UNIVERSITY OF PRETORIA
YUNIBESITHI YA PRETORIA

spent working on and lead to the acquisition of valuable technical skills. As is the nature of experimental work, however, an experimental setup is never completed, only abandoned – if only for the purpose of completing this work. That being said, the setup is at this time already being expanded upon. Two of the additions include the development of single particle tracking capability, as well as super-resolution microscopy through the use of a spatial light modulator.

From the data that was collected it was seen that a second photoprotective energy quenching mechanism in the major light harvesting antenna of higher plants could possibly be activated by low-pH induced structural conformation, where excitation are quenched before reaching the terminal emitter. Additionally, a possible relationship between an increased switching between fluorescence intermittency induced *on* and *off* states and the presence of intermediate fluorescence intensity states. However, the statistical approach used here was inadequate to draw concrete conclusions, and future work will include the development of a more robust and insightful statistical method of categorisation.

UNIVERSITEIT VAN PRETORIA
UNIVERSITY OF PRETORIA
YUNIBESITHI YA PRETORIA

Appendices

UNIVERSITEIT VAN PRETORIA
UNIVERSITY OF PRETORIA
YUNIBESITHI YA PRETORIA

Appendix A

List of Abbreviations

ADP	Adenosine diphosphate
AOTF	Acousto-optic tuneable filter
ATP	Adenosine triphosphate
BH	Becker Hickl
BS	Beam splitter
ChlA & B	Chlorophyll A & B
CCD	Charge coupled device
CP	Confocal pinhole
DLL	Dynamic link library
EET	Excited energy transfer
EMCCD	Electron multiplying CCD
FIFO	First in, first out
FF	Fluorescence filter
FWHM	Full-width at half maximum
GUI	Graphical user interface
LHCII	Light harvesting complex II
LPF	Longpass filter
NA	Numerical aperture
$NADP^+$	Nicotinamide adenine dinucleotide phosphate
NADPH	Nicotinamide adenine dinucleotide phosphate-oxidase
NPQ	Non-photochemical quenching
OEC	Oxygen evolving complex
PLL	Poly-L-lysine
PSI & II	Photosystem I & II
PSF	Point spread function
RS	Raster scan
RC	Reaction centre
SF	Spatial filter
SMS	Single molecule spectroscopy
SNR	Signal-to-noise ratio
SPAD	Single photon avalanche diode
SPT	Single particle tracking
TCSPC	Time correlated single photon counting
TTL	Transistor-transistor logic
qE	Energy dependent component of NPQ
USB	Universal serial bus

Appendix B

Setup Specifications

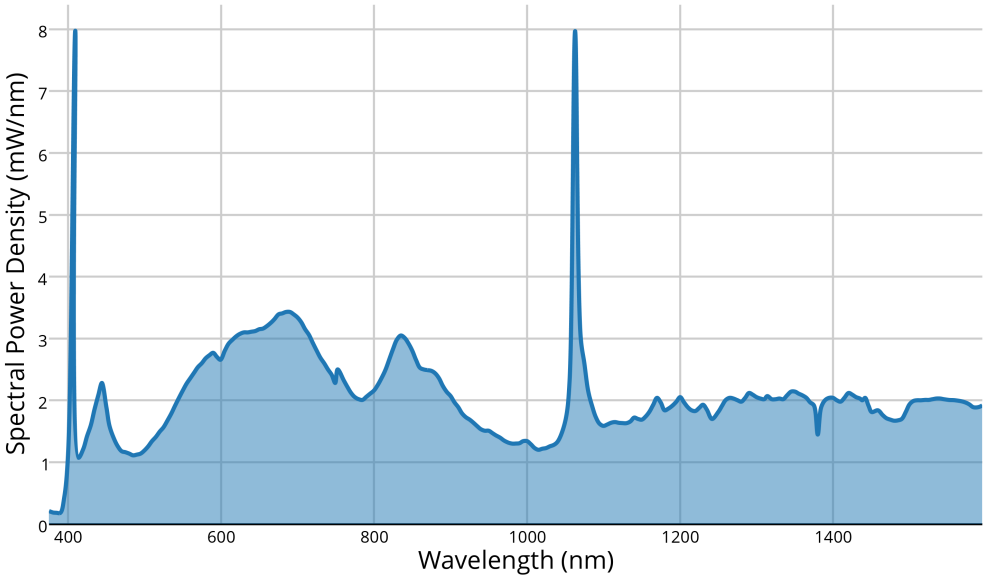

Figure B.1: Fianium PP-400-4 supercontinuum laser emission spectral density.

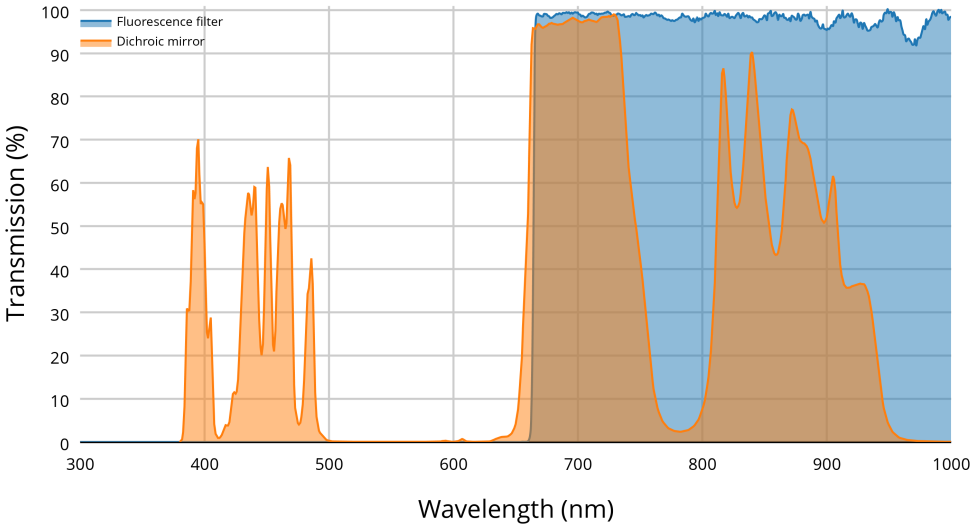

Figure B.2: Chroma EM ET665lp fluorescence filter and DM T660lpxrxt dichroic beam splitter transmission spectrum. The cut-off wavelengths of the fluorescence filter and dichroic beam splitter are 665 nm and 665 nm respectfully.

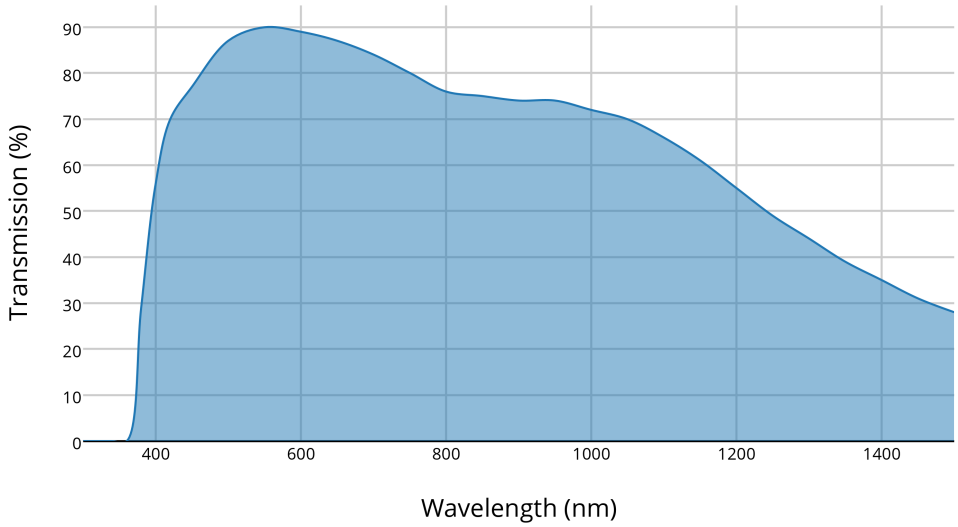

Figure B.3: Nikon CFI Plan Apochromat Lambda 100X oil immersion objective transmission spectrum.

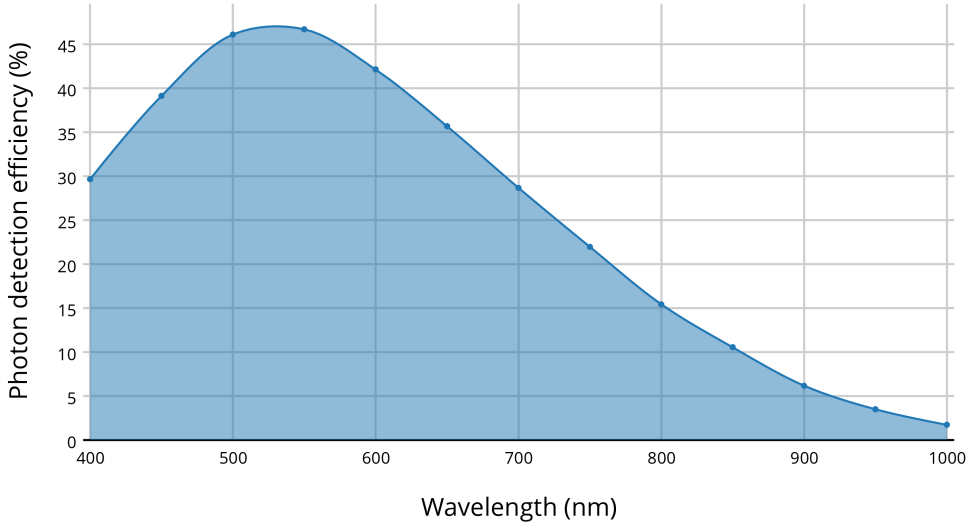

Figure B.4: Micro Photon Devices PD-050-CTE 50 µm by 50 µm Peltier cooled photon detection efficiency as a function of wavelength. Taken from Giudice et al. [52]

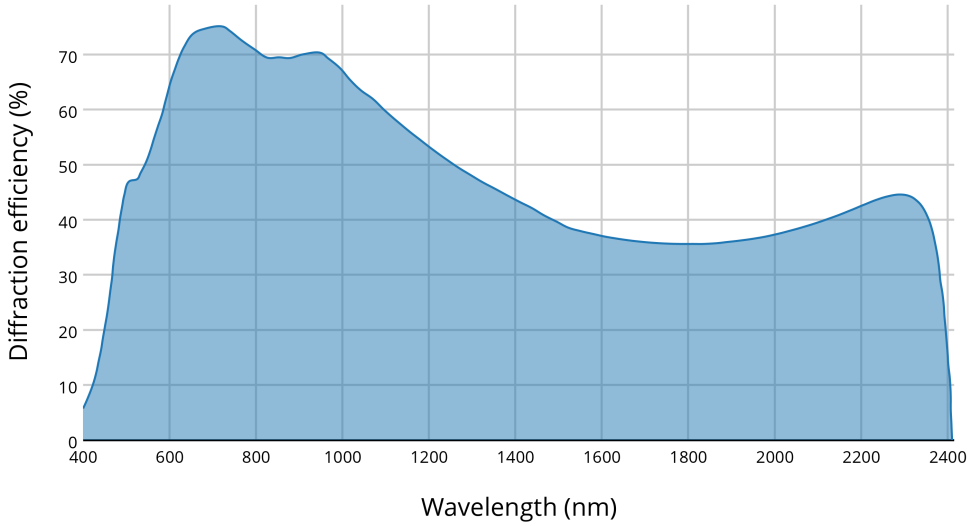

Figure B.5: Optometrics 3-8880 gold coated diffraction grating efficiency as function of wavelength.

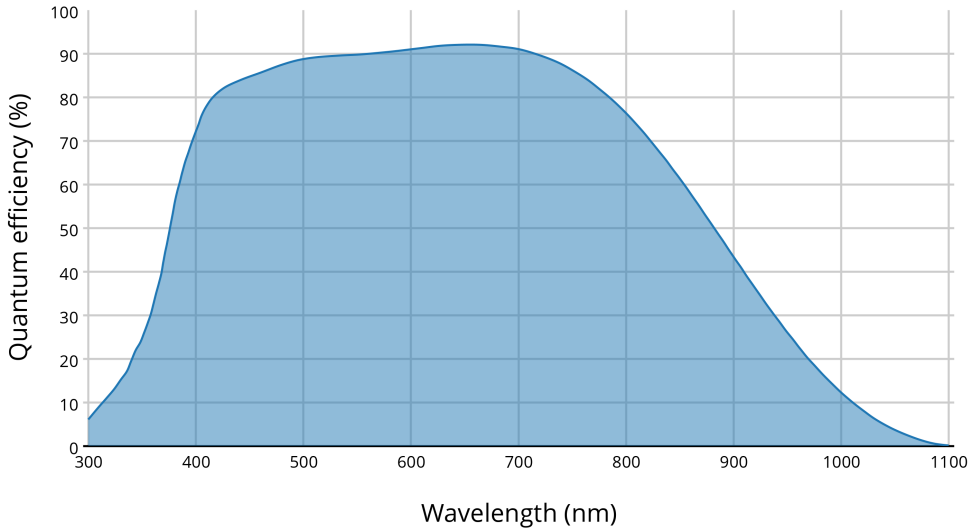

Figure B.6: Andor iXon$_3$ 897 (DU-897E-CS0-EXF) EMCCD detection quantum efficiency as function of wavelength.

UNIVERSITEIT VAN PRETORIA
UNIVERSITY OF PRETORIA
YUNIBESITHI YA PRETORIA

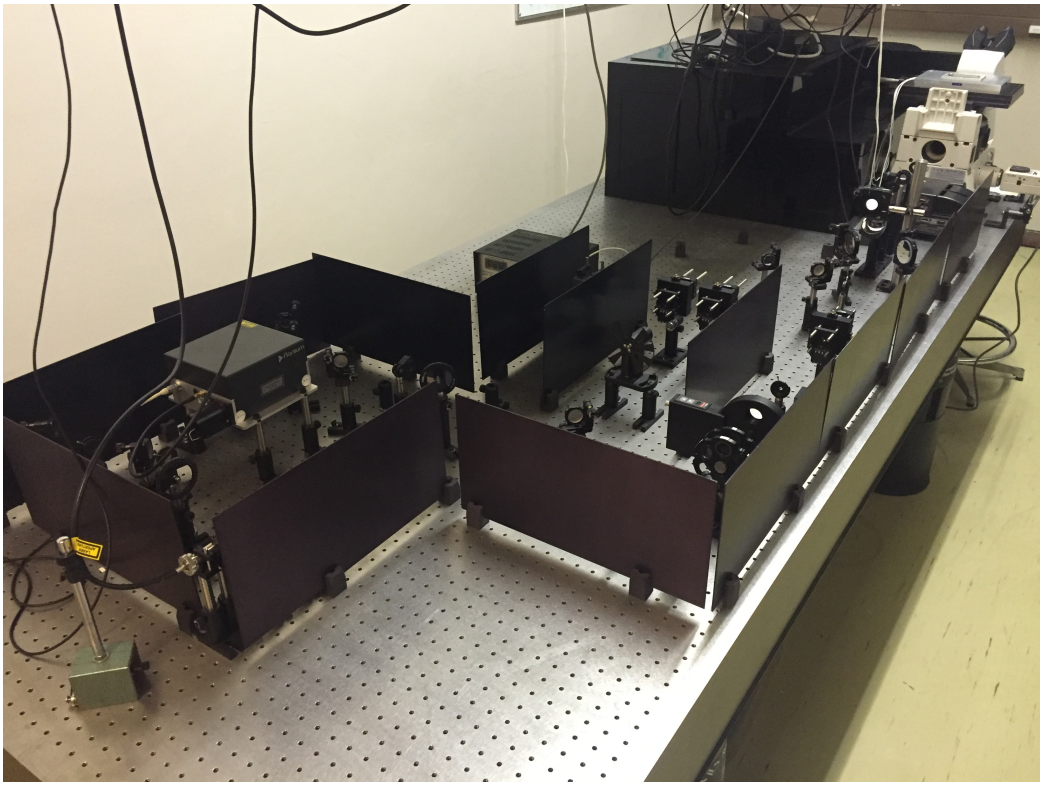

Figure B.7: Photo of experimental setup.

UNIVERSITEIT VAN PRETORIA
UNIVERSITY OF PRETORIA
YUNIBESITHI YA PRETORIA

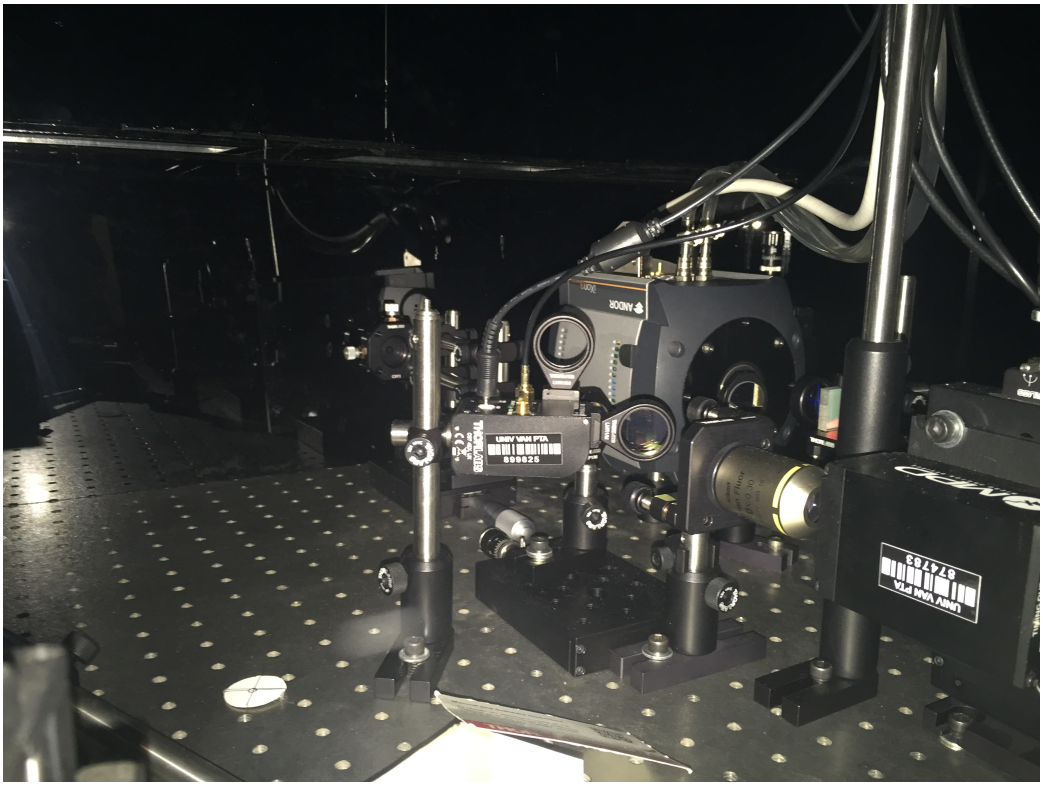

Figure B.8: Photo of the detection part of the experimental setup.

Appendix C

Software Code Examples

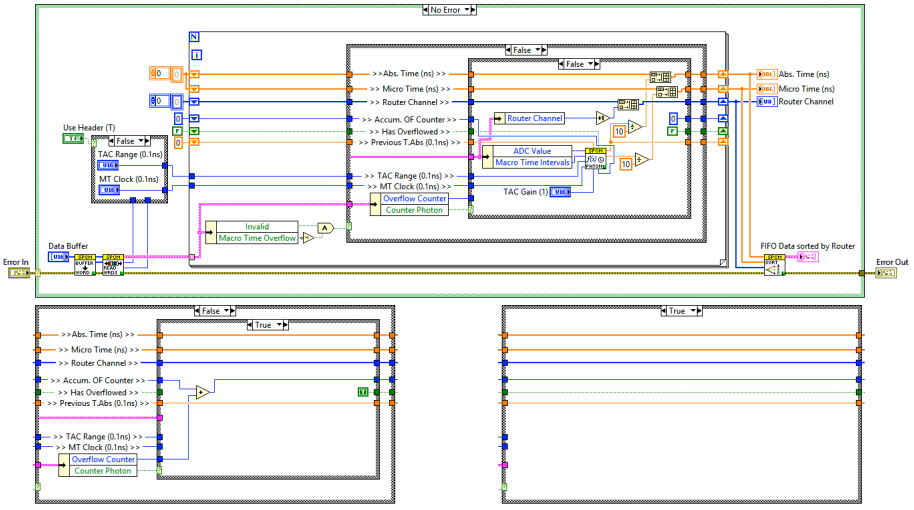

(a) LabVIEW™'SPCM Data Extraction.vi' code.

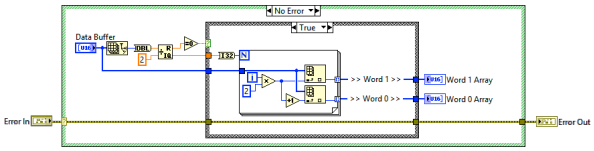

(b) LabVIEW™'SPCM Buffer to Words.vi' code.

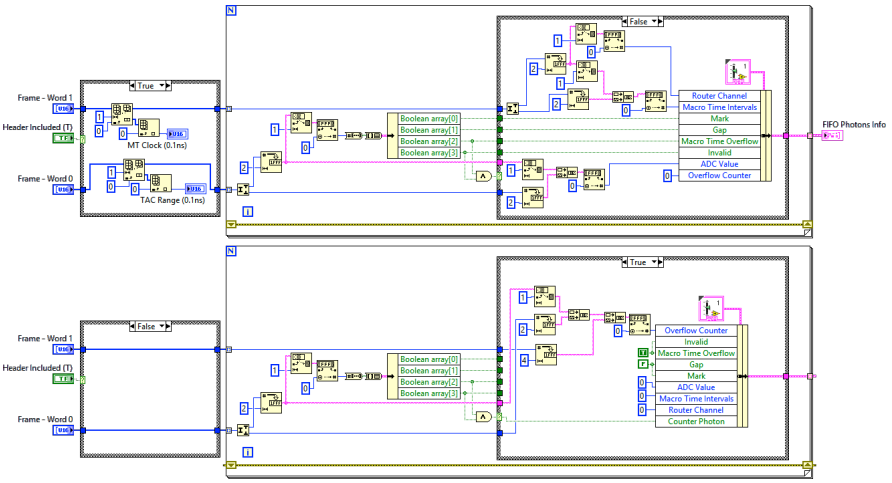

(c) LabVIEW™'SPCM Read Words - Array.vi' code.

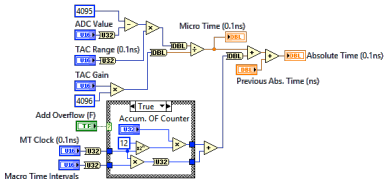

(d) LabVIEW™'SPCM Calculate Photon Times.vi' code.

Figure C.1: Screen captures of the LabVIEW™ code for the extraction of photon times.

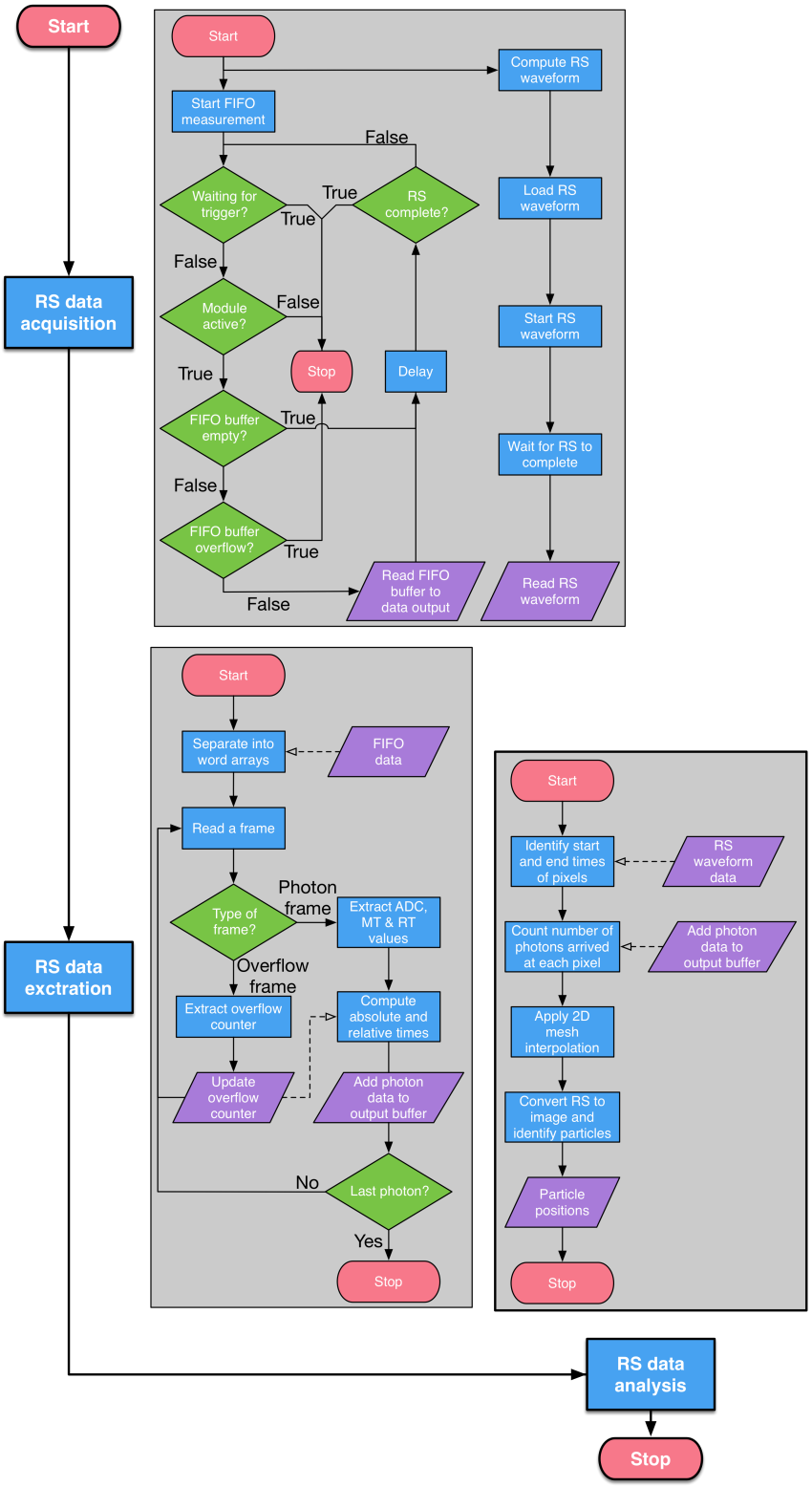

Figure C.2: Complete raster scan flow diagram.

UNIVERSITEIT VAN PRETORIA
UNIVERSITY OF PRETORIA
YUNIBESITHI YA PRETORIA

Bibliography

[1] A. Gando, Y. Gando, K. Ichimura, H. Ikeda, K. Inoue *et al.*, "Partial radiogenic heat model for earth revealed by geoneutrino measurements," *Nature Geoscience*, vol. 4, no. 9, pp. 647–651, 2011.

[2] L.-H. Lin, P.-L. Wang, D. Rumble, J. Lippmann-Pipke, E. Boice *et al.*, "Long-term sustainability of a high-energy, low-diversity crustal biome," *Science*, vol. 314, no. 5798, pp. 479–82, 2006. [Online]. Available: http://science.sciencemag.org/content/314/5798/479.abstract

[3] N. Armaroli and V. Balzani, "The future of energy supply: Challenges and opportunities," *Angewandte Chemie - International Edition*, vol. 46, no. 1-2, pp. 52–66, 2007.

[4] D. O. Hall and K. Rao, *Photosynthesis*. Cambridge University Press, 1999. [Online]. Available: https://books.google.com/books?id=6F7yuf1Sj30C{&}pgis=1

[5] L. Mustárdy and G. Garab, "Granum revisited. A three-dimensional model - Where things fall into place," *Trends in Plant Science*, vol. 8, no. 3, pp. 117–122, 2003.

UNIVERSITEIT VAN PRETORIA
UNIVERSITY OF PRETORIA
YUNIBESITHI YA PRETORIA

[6] J. P. Dekker and E. J. Boekema, "Supramolecular organization of thylakoid membrane proteins in green plants," *Biochimica et biophysica acta*, vol. 1706, no. 1-2, pp. 12–39, 2005.

[7] D. J. Paolillo, "The three-dimensional arrangement of intergranal lamellae in chloroplasts," *Journal of cell science*, vol. 6, no. 1, pp. 243–255, 1970.

[8] P. Horton, A. V. Ruban, and R. G. Walters, "Regulation of light harvesting in green plants," in *Annual Review of Plant Physiology and Plant Molecular Biology*, 1996, vol. 47, no. 1, pp. 655–684.

[9] C. Laloi and M. Havaux, "Key players of singlet oxygen-induced cell death in plants," *Frontiers in plant science*, vol. 6, no. February, p. 39, 2015. [Online]. Available: http://www.pubmedcentral.nih.gov/articlerender.fcgi?artid=4316694{&}tool=pmcentrez{&}rendertype=abstract

[10] R. Kouřil, J. P. Dekker, and E. J. Boekema, "Supramolecular organization of photosystem II in green plants," *Biochimica et biophysica acta*, vol. 1817, no. 1, pp. 2–12, 2012. [Online]. Available: http://www.ncbi.nlm.nih.gov/pubmed/21723248

[11] S. Caffarri, R. Kouřil, S. Kereïche, E. J. Boekema, and R. Croce, "Functional architecture of higher plant photosystem II supercomplexes," *The EMBO journal*, vol. 28, no. 19, pp. 3052–3063, 2009.

[12] A. Guskov, J. Kern, A. Gabdulkhakov, M. Broser, A. Zouni, and W. Saenger, "Cyanobacterial photosystem II at 2.9 Å resolution and the role of quinones, lipids, channels and chloride," *Nature structural & molecular biology*, vol. 16, no. 3, pp. 334–342, 2009.

[13] F. Müh, T. Renger, and A. Zouni, "Crystal structure of cyanobacterial photosystem II at 3.0 Å resolution: A closer look at the antenna system and the

UNIVERSITEIT VAN PRETORIA
UNIVERSITY OF PRETORIA
YUNIBESITHI YA PRETORIA

small membrane-intrinsic subunits," in *Plant Physiology and Biochemistry*, 2008, vol. 46, no. 3, pp. 238–264.

[14] B. Loll, J. Kern, W. Saenger, A. Zouni, and J. Biesiadka, "Towards complete cofactor arrangement in the 3.0 Å resolution structure of photosystem II," *Nature*, vol. 438, no. 7070, pp. 1040–1044, 2005.

[15] N. Kamiya and J.-R. Shen, "Crystal structure of oxygen-evolving photosystem II from Thermosynechococcus vulcanus at 3.7 Å resolution," *Proceedings of the National Academy of Sciences of the United States of America*, vol. 100, no. 1, pp. 98–103, 2003.

[16] A. Zouni, H. T. Witt, J. Kern, P. Fromme, N. Krauss *et al.*, "Crystal structure of photosystem II from Synechococcus elongatus at 3.8 Å resolution," *Nature*, vol. 409, no. 6821, pp. 739–743, 2001.

[17] X. Wei, X. Su, P. Cao, X. Liu, W. Chang *et al.*, "Structure of spinach photosystem II-âĂŞLHCII supercomplex at 3.2 Å resolution," *Nature*, vol. 1, pp. 1–18, 2016. [Online]. Available: http://dx.doi.org/10.1038/nature18020http://www.nature.com/doifinder/10.1038/nature18020

[18] Z. Liu, H. Yan, K. Wang, T. Kuang, J. Zhang *et al.*, "Crystal structure of spinach major light-harvesting complex at 2.72 Å resolution," *Nature*, vol. 428, no. 6980, pp. 287–292, 2004.

[19] X. Pan, M. Li, T. Wan, L. Wang, C. Jia *et al.*, "Structural insights into energy regulation of light-harvesting complex CP29 from spinach," *Nature structural & molecular biology*, vol. 18, no. 3, pp. 309–315, 2011.

[20] J. Standfuss, A. C. Terwisscha van Scheltinga, M. Lamborghini, and W. Kühlbrandt, "Mechanisms of photoprotection and nonphotochemical

UNIVERSITEIT VAN PRETORIA
UNIVERSITY OF PRETORIA
YUNIBESITHI YA PRETORIA

quenching in pea light-harvesting complex at 2.5 Å resolution," *The EMBO journal*, vol. 24, no. 5, pp. 919–928, 2005.

[21] H. Yan, P. Zhang, C. Wang, Z. Liu, and W. Chang, "Two lutein molecules in LHCII have different conformations and functions: insights into the molecular mechanism of thermal dissipation in plants," *Biochemical and biophysical research communications*, vol. 355, no. 2, pp. 457–463, 2007.

[22] T. P. J. Krüger, C. Ilioaia, M. P. Johnson, A. V. Ruban, and R. Van Grondelle, "Disentangling the low-energy states of the major light-harvesting complex of plants and their role in photoprotection," *Biochimica et Biophysica Acta - Bioenergetics*, vol. 1837, no. 7, pp. 1027–1038, 2014. [Online]. Available: http://dx.doi.org/10.1016/j.bbabio.2014.02.014

[23] T. P. J. Krüger, C. Ilioaia, L. Valkunas, and R. Van Grondelle, "Fluorescence intermittency from the main plant light-harvesting complex: Sensitivity to the local environment," *Journal of Physical Chemistry B*, vol. 115, no. 18, pp. 5083–5095, 2011.

[24] L. Valkunas, J. Chmeliov, T. P. J. Krüger, C. Ilioaia, and R. Van Grondelle, "How photosynthetic proteins switch," *Journal of Physical Chemistry Letters*, vol. 3, no. 19, pp. 2779–2784, 2012.

[25] V. I. Novoderezhkin, M. A. Palacios, H. Van Amerongen, and R. Van Grondelle, "Excitation dynamics in the LHCII complex of higher plants: Modeling based on the 2.72 Å crystal structure," *Journal of Physical Chemistry B*, vol. 109, no. 20, pp. 10 493–10 504, 2005.

[26] R. van Grondelle and V. I. Novoderezhkin, "Energy transfer in photosynthesis: experimental insights and quantitative models," *Physical*

UNIVERSITEIT VAN PRETORIA
UNIVERSITY OF PRETORIA
YUNIBESITHI YA PRETORIA

Chemistry Chemical Physics, vol. 8, no. 7, pp. 793–807, 2006. [Online]. Available: http://www.ncbi.nlm.nih.gov/pubmed/16482320

[27] T. P. J. Krüger, C. Ilioaia, M. P. Johnson, A. V. Ruban, E. Papagiannakis *et al.*, "Controlled disorder in plant light-harvesting complex II explains its photoprotective role," *Biophysical Journal*, vol. 102, no. 11, pp. 2669–2676, 2012.

[28] T. Basché, S. Kummer, and C. Bräuchle, "Direct spectroscopic observation of quantum jumps of a single molecule," *Nature*, vol. 373, no. 6510, pp. 132–134, 1995.

[29] M. Nirmal, B. O. Dabbousi, M. G. Bawendi, J. J. Macklin, J. K. Trautman *et al.*, "Fluorescence intermittency in single cadmium selenide nanocrystals," *Nature*, vol. 383, no. 6603, pp. 802–804, 1996. [Online]. Available: http://www.nature.com/doifinder/10.1038/383802a0

[30] R. M. Dickson, A. B. Cubitt, R. Y. Tsien, and W. E. Moerner, "On/off blinking and switching behaviour of single molecules of green fluorescent protein," *Nature*, vol. 388, no. 6640, pp. 355–358, 1997.

[31] M. A. Palacios, F. L. De Weerd, J. A. Ihalainen, R. Van Grondelle, and H. Van Amerongen, "Superradiance and exciton (de)localization in light-harvesting complex II from green plants?" *Journal of Physical Chemistry B*, vol. 106, no. 22, pp. 5782–5787, 2002.

[32] M. Böhmer and J. Enderlein, "Single Molecule Detection on Surfaces with the Confocal Laser Scanning Microscope," in *Single Molecule Detection in Solution*, C. Zander, J. Enderlein, and R. A. Keller, Eds. Wiley-VCH Verlag GmbH & Co. KGaA, 2002, pp. 145–183. [Online]. Available: http://dx.doi.org/10.1002/3527600809.ch5

UNIVERSITEIT VAN PRETORIA
UNIVERSITY OF PRETORIA
YUNIBESITHI YA PRETORIA

[33] T. P. J. Krüger, V. I. Novoderezhkin, C. Ilioaia, and R. Van Grondelle, "Fluorescence spectral dynamics of single LHCII trimers," *Biophysical Journal*, vol. 98, no. 12, pp. 3093–3101, 2010.

[34] E. Brooks Shera, N. K. Seitzinger, L. M. Davis, R. A. Keller, and S. A. Soper, "Detection of single fluorescent molecules," *Chemical Physics Letters*, vol. 174, no. 6, pp. 553–557, 1990.

[35] W. E. Moerner, "Finding a single molecule in a haystack: Optical detection and spectroscopy of single absorbers in solids," *Analytical Chemistry*, vol. 61, no. 21, pp. 1217–1223, 1989.

[36] L.-Q. Li and L. M. Davis, "Single photon avalanche diode for single molecule detection," *Review of Scientific Instruments*, vol. 37388, no. January, pp. 1524–1529, 1993. [Online]. Available: http://ieeexplore.ieee.org/xpls/abs{_}all.jsp?arnumber=4991058

[37] S. A. Soper, Q. L. Mattingly, and P. Vegunta, "Photon burst detection of single ear-infrared fluorescent molecules," *Analytical Chemistry*, vol. 65, no. 6, pp. 740–747, 1993.

[38] S. Cova, M. Ghioni, A. Lacaita, C. Samori, and F. Zappa, "Avalanche photodiodes and quenching circuits for single-photon detection," *Applied optics*, vol. 35, no. 12, pp. 1956–1976, 1996.

[39] H. H. Robinson and C. F. Yocum, "Cyclic photophosphorylation reactions catalyzed by ferredoxin, methyl viologen and anthraquinone sulfonate. Use of photochemical reactions to optimize redox poising," *BBA - Bioenergetics*, vol. 590, no. 1, pp. 97–106, 1980.

[40] D. A. Berthold, G. T. Babcock, and C. F. Yocum, "A highly resolved, oxygen-evolving photosystem II preparation from spinach

UNIVERSITEIT VAN PRETORIA
UNIVERSITY OF PRETORIA
YUNIBESITHI YA PRETORIA

thylakoid membranes," *FEBS Letters*, vol. 134, no. 2, pp. 231–234, nov 1981. [Online]. Available: http://www.sciencedirect.com/science/article/pii/0014579381806084

[41] P. J. van Leeuwen, M. C. Nieveen, E. J. van de Meent, J. P. Dekker, and H. J. van Gorkom, "Rapid and simple isolation of pure photosystem II core and reaction center particles from spinach," *Photosynthesis Research*, vol. 28, no. 3, pp. 149–153, 1991.

[42] H. Van Roon, J. F. L. Van Breemen, F. L. De Weerd, J. P. Dekker, and E. J. Boekema, "Solubilization of green plant thylakoid membranes with n-dodecyl-α,D-maltoside. Implications for the structural organization of the Photosystem II, Photosystem I, ATP synthase and cytochrome b6f complexes," *Photosynthesis Research*, vol. 64, no. 2-3, pp. 155–166, 2000.

[43] R. J. Porra, W. A. Thompson, and P. E. Kriedemann, "Determination of accurate extinction coefficients and simultaneous equations for assaying chlorophylls a and b extracted with four different solvents: verification of the concentration of chlorophyll standards by atomic absorption spectroscopy," *BBA - Bioenergetics*, vol. 975, no. 3, pp. 384–394, 1989.

[44] J. M. Briantais, C. Vernotte, M. Picaud, and G. H. Krause, "A quantitative study of the slow decline of chlorophyll a fluorescence in isolated chloroplasts," *BBA - Bioenergetics*, vol. 548, no. 1, pp. 128–138, 1979.

[45] A. Krieger, I. Moya, and E. Weis, "Energy-dependent quenching of chlorophyll a fluorescence: effect of pH on stationary fluorescence and picosecond-relaxation kinetics in thylakoid membranes and Photosystem II preparations," *BBA - Bioenergetics*, vol. 1102, no. 2, pp. 167–176, 1992.

[46] D. Rees, G. Noctor, A. V. Ruban, J. Crofts, A. Young, and P. Horton, "pH dependent chlorophyll fluorescence quenching in spinach thylakoids from light treated or dark adapted leaves," *Photosynthesis Research*, vol. 31, no. 1, pp. 11–19, 1992.

[47] T. P. J. Krüger, C. Ilioaia, and R. van Grondelle, "Fluorescence intermittency from the main plant light-harvesting complex: Resolving shifts between intensity levels," *The Journal of Physical Chemistry B*, vol. 115, no. 18, pp. 5071–5082, 2011. [Online]. Available: http://pubs.acs.org/doi/abs/10.1021/jp201609c

[48] J. Chmeliov, L. Valkunas, T. P. J. Krüger, C. Ilioaia, and R. van Grondelle, "Fluorescence blinking of single major light-harvesting complexes," *New Journal of Physics*, vol. 15, 2013.

[49] T. P. J. Krüger and R. van Grondelle, "Design principles of natural light-harvesting as revealed by single molecule spectroscopy," *Physica B: Condensed Matter*, vol. 480, pp. 7–13, jan 2016. [Online]. Available: http://www.sciencedirect.com/science/article/pii/S0921452615301551

[50] J. M. Gruber, S. Scheidelaar, H. van Roon, J. P. Dekker, J. A. Killian, and R. van Grondelle, "Photophysics in single light-harvesting complexes II: from micelle to native nanodisks," vol. 9714, p. 97140A, 2016. [Online]. Available: http://proceedings.spiedigitallibrary.org/proceeding.aspx?doi=10.1117/12.2211588

[51] G. S. Schlau-Cohen, H. Y. Yang, T. P. J. Krüger, P. Xu, M. Gwizdala *et al.*, "Single-molecule identification of quenched and unquenched states of LH-CII," *Journal of Physical Chemistry Letters*, vol. 6, no. 5, pp. 860–867, 2015.

[52] A. Giudice, M. Ghioni, R. Biasi, F. Zappa, S. Cova *et al.*, "High-rate photon counting and picosecond timing with silicon-SPAD based compact detector modules," *Journal of Modern Optics*, vol. 54, no. 2-3, pp. 225–237, 2007.

UNIVERSITEIT VAN PRETORIA
UNIVERSITY OF PRETORIA
YUNIBESITHI YA PRETORIA

"Admiration & love, to which all knowledge truly vital must tend, are felt by men of real genius in proportion as their discoveries in Natural Philosophy are enlarged; and the beauty in form of a plant or an animal is not made less but more apparent as whole by a more accurate insight into its constituent properties & powers."

- William Wordsworth